

# **An Investigation of Maximum Brake Torque Timing based on Ionization Current Feedback**

**Master's thesis**  
performed in **Vehicular Systems**  
by

**Janek Magnusson**

Reg nr: LiTH-ISY-EX--06/3809--SE

April 13, 2007



# **An investigation of Maximum Brake Torque Timing based on Ionization Current Feedback**

**Master's thesis**  
performed in **Vehicular Systems,**  
**Dept. of Electrical Engineering**  
at **Linköping University**  
by

**Janek Magnusson**


Reg nr: LiTH-ISY-EX--06/3809--SE

Supervisors: **Ylva Nilsson and Marcus Klein**  
Linköping University  
**Richard Backman**  
GM Powertrain Sweden

Examiner: **Associate Professor Lars Eriksson**  
Linköping University

Linköping, April 13, 2007



<b>Presentationsdatum</b> 2007-04-13 <b>Publiceringsdatum (elektronisk version)</b> _____	<b>Institution och avdelning</b> <b>Institutionen för systemteknik</b>  <b>Department of Electrical Engineering</b>	 <b>Linköpings universitet</b>
--	--	--

<b>Språk</b> _____ Svenska <input checked="" type="checkbox"/> Annat (ange nedan)  Engelska _____ <b>Antal sidor</b> 49 _____	<b>Typ av publikation</b> _____ Licentiatavhandling <input checked="" type="checkbox"/> Examensarbete _____ C-uppsats _____ D-uppsats _____ Rapport _____ Annat (ange nedan) _____	<b>ISBN (licentiatavhandling) —</b>  <b>ISRN LITH-ISY-EX--06/3809--SE</b>  <b>Serietitel (licentiatavhandling)</b> —  <b>Serienummer/ISSN (licentiatavhandling)</b> —
---	---	---

<b>URL för elektronisk version</b> <a href="http://www.vehicular.isy.liu.se">http://www.vehicular.isy.liu.se</a>
---

<b>Publikationens titel</b> An Investigation of Maximum Brake Torque Timing based on Ionization Current Feedback Tändningstidpunkt för maximalt arbete baserat på jonströmsåterkoppling  <b>Författare</b> Janek Magnusson
---

<b>Sammanfattning</b> <p>For every operating condition of an internal combustion engine there exists an optimal spark timing, called maximum brake torque (MBT), which maximises the output torque and the efficiency of the engine. Traditionally MBT timing is implemented as an open-loop control where the ignition timing is found by using a combination of static lookup tables and sensor information. With a direct closed-loop control from the combustion process the performance of internal combustion engines could be improved. The thesis investigates if it is possible to estimate the MBT timing from the ionization current for every operating condition of a spark ignited engine where the operating conditions are defined by the engine parameters <math>\lambda</math>, internal exhaust gas recirculation, engine load, engine speed and spark advance.</p> <p>First an investigation of how much loss of torque an error from the MBT position corresponds to is made. Then the influence of the engine parameters on the shape of the ionization current was studied. Last different peak pressure position (PPP) estimating algorithms are presented and a new technique is developed where an engine operating point dependant part of the ionization current is used depending on the current operating condition of the engine. Two of the presented PPP estimating algorithms are then complemented with this technique and the results look promising.</p>
--

<b>Nyckelord</b> MBT timing, maximum brake torque, spark advance, PPP, ion current
---



# Abstract

For every operating condition of an internal combustion engine there exists an optimal spark timing, called maximum brake torque (MBT), which maximises the output torque and the efficiency of the engine. Traditionally MBT timing is implemented as an open-loop control where the ignition timing is found by using a combination of static lookup tables and sensor information. With a direct closed-loop control from the combustion process the performance of internal combustion engines could be improved. The thesis investigates if it is possible to estimate the MBT timing from the ionization current for every operating condition of a spark ignited engine where the operating conditions are defined by the engine parameters  $\lambda$ , internal exhaust gas recirculation, engine load, engine speed and spark advance.

First an investigation of how much loss of torque an error from the MBT position corresponds to is made. Then the influence of the engine parameters on the shape of the ionization current was studied. Last different peak pressure position (PPP) estimating algorithms are presented and a new technique is developed where an engine operating point dependant part of the ionization current is used depending on the current operating condition of the engine. Two of the presented PPP estimating algorithms are then complemented with this technique and the results look promising.





# Acknowledgement

I would especially like to thank my supervisor Richard Backman for his patience and for taking me in at GM Powertrain Sweden. The summer 2005 in Södertälje will always stay in my mind. I would also like to thank my supervisors Ylva Nilsson and Marcus Klein for your patience and guidance. Thanks to Martin Gunnarsson for helping me in the engine laboratory and Ulf Holmberg for taking your time to answer my questions. Finally I would like to express my love and appreciation for my family, friends and for Eva.

Janek Magnusson  
Linköping, April 2007



# Contents

Chapter 1 Introduction .....	1
1.2 Thesis outline .....	2
1.3 Experimental setup .....	2
Chapter 2 The cylinder pressure .....	3
2.1 The four stroke engine .....	3
2.2 SA and MBT timing .....	5
2.3 Combustion descriptors .....	8
2.3.1 PPP .....	8
2.3.2 50%MFB .....	8
2.3.3 MAMFB .....	10
2.3.4 Illustrated examples .....	10
2.4 %MBT performance .....	11
Chapter 3 The ionization current .....	15
3.1 Origin and measurement .....	15
3.2 Cycle-to-cycle variations .....	15
3.3 The three phases .....	16
3.3.1 Ignition phase .....	17
3.3.2 Flame front phase .....	18
3.3.3 Post flame phase .....	18
3.4 Influence of engine operating parameters .....	19
3.4.1 $\lambda$ .....	20
3.4.2 EGR .....	22
3.4.3 Engine load .....	23
3.4.4 Engine speed .....	24
3.4.6 SA .....	26
3.5 Influence of fuel additives .....	27
Chapter 4 Implementation, estimation and result .....	29
4.1 PPP estimating algorithms .....	29
4.1.1 ANN .....	29
4.1.2 Gaussian fit .....	30
4.1.3 SQUAD aka Peakfinder .....	30
4.1.4 DD .....	31
4.2 Implementation .....	31
4.2.1 SQUAD .....	31
4.2.2 DD .....	32
4.2.3 Improvement .....	33
4.3 Parameter estimation .....	35
4.4 Result .....	39
4.5 Robustness .....	40
4.5.1 $\lambda$ sweep .....	40
4.5.2 EGR sweep .....	41
Chapter 5 Summary and conclusions .....	43
5.1 Future work .....	44
References .....	47

# Abbreviations

AFR	Air/fuel ratio
AMFB	Acceleration of mass fraction burned
ANN	Artificial neural network
ATDC	After top dead center
BDC	Bottom dead center, engine crank position at $\pm 180$ CAD
CAD	Crank angle degree
DD	Double difference
ECU	Electronic control unit
EGR	Exhaust gas recirculation
eMOP	Exhaust maximum opening position
iMOP	Intake maximum opening position
MAMFB	Maximum acceleration of mass fraction burned
MBT	Maximum brake torque
MFB	Mass fraction burned
PPP	Pressure peak position
RMS	Root mean square
SA	Spark advance, the engine crank position when the spark plug ignites the air-fuel mixture contained in the cylinder
SI	Spark ignited
SQUAD	Sliding quadratic fit
TDC	Top dead center, engine crank position at 0 and $\pm 360$ CAD

# Chapter 1

## Introduction

For internal combustion engines there exists an optimal spark timing, called maximum brake torque timing, for each operating condition which maximises the output torque. An earlier or later ignition timing from this optimum will result in a lower output torque. It is desirable to operate an engine at maximum brake torque (MBT) to keep the fuel consumption down and to maximise the efficiency of the engine. Traditionally in modern cars MBT timing is implemented as an open-loop control which depends on static lookup tables. The values of these tables have experimentally been determined by conducting time consuming spark sweeps for a number of operating conditions. Open-loop control algorithms are then used to determine a spark timing by using a combination of these tables and information from sensors such as engine load, engine speed, throttle angle, coolant temperature and atmospheric pressure. A problem with this approach is that several factors like engine aging and diversities, fuel composition and environmental disturbances like humidity which also affect the optimum spark timing are ignored. As a result of this, the engine is not running at its optimum. One way of improving the performance of the engine is to complement the MBT timing with feedback information from the combustion process. The most desirable would be to use information from a cylinder pressure sensor since it directly reflects the ongoing combustion process. But due to their high cost and the added complexity for design and manufacturing they are not conceivable for mass production yet. An alternative is to make use of the already existing spark plug to perform measurements of the current flowing through the ionized combustion chamber. Using the spark plug as a sensor has proven cost effective and several ionization current systems are already in use in production cars today; for example in misfire detection and cam phase sensing applications. Since all the hardware already is implemented, adding an ionization current based spark advance (SA) system only requires some additional signal interpretation by the electronic control unit (ECU). However, there exist some drawbacks with ionization current measurements. The quality of the signal is quite poor and the shape is influenced by several parameters such as electronic design, sensor location, spark plug geometry, fuel additives and different engine operating parameters. This thesis investigates if it is possible to estimate the MBT timing from the complex ionization current for every operating condition of a spark ignited (SI) engine where the operating conditions are defined by the engine parameters  $\lambda$ , internal exhaust gas recirculation (EGR), engine load, engine speed and SA.

## 1.2 Thesis outline

### Chapter 2 – The cylinder pressure

The four stroke SI engine and the importance of MBT timing are explained. The combustion descriptors PPP, 50%MFB and MAMFB are introduced and an investigation of how much loss of torque a SA and PPP error in CAD from the MBT position corresponds to is made.

### Chapter 3 – Ionization current

The ionization current is first described and then the influence of fuel additives and the engine operating parameters on the amplitude and phasing of the ionization current are investigated for two different ignition systems.

### Chapter 4 – Implementation, estimation and result

Four different PPP estimating algorithms and their different approaches to estimate the PPP from the post flame peak of the ionization current are presented. A new technique is then developed where an engine operating point dependant part of the ionization current is used when estimating the PPP. Two of the presented algorithms are then complemented with this technique and evaluated.

### Chapter 5 – Summary and conclusions

Last a summary and the conclusions of the thesis is presented together with the suggested areas for future work.

## 1.3 Experimental setup

All of the measurements in this thesis were performed in the research laboratory at the division of Vehicular Systems at the Department of Electrical Engineering, Linköping University. The measurements were made on a L850 engine from SAAB. It is a spark ignited, four stroke, two liters, turbo charged, piston engine with four cylinders. The engine is controlled by the ECU. Two different inductive ignition systems were used; a Mecel system in cylinder 1 with a short ignition duration and a SAAB system in cylinder 2 with a long ignition duration. Measurements of the ionization current and cylinder pressure were made simultaneous in both cylinders. The cylinder pressure was measured with an AVL GU21D.

## Chapter 2

### The cylinder pressure

To be able to understand the importance of maximum brake torque (MBT) timing, basic understanding of the four stroke engine and the effect of spark advance (SA) on the engine brake torque is required. After the basics have been covered, three combustion descriptors which can be used for closed-loop control of the SA for MBT timing are presented. Last an investigation of how much loss of torque an error from the MBT position corresponds to is made.

#### 2.1 The four stroke engine

The most commonly used engine in passenger cars today is the four stroke spark ignited (SI) engine. The engine uses air and fuel to generate power and emissions as can be seen in figure 2.1. A full combustion cycle requires four strokes of a cylinder's piston, corresponding to two revolutions of the crankshaft to complete. The four strokes intake, compression, expansion and exhaust are illustrated in figure 2.2 and explained below. The angle between the crankshaft and the axis of the cylinder will be referred to as the crank angle degree (CAD). The convention will be to have it negative during the intake and compression stroke and positive during the expansion and exhaust stroke. The top CAD position is called the top dead center (TDC) and the bottom CAD position is called the bottom dead center (BDC).

Intake stroke:

During the intake stroke the air-fuel mixture is drawn into the cylinder from the intake manifold due to the pressure difference generated by the downwards movement of the piston from TDC to BDC.

Compression stroke:

As the piston moves upwards to TDC the pressure of the air-fuel mixture contained in the cylinder steadily increases. When the piston reaches a certain point before TDC, called spark advance (SA), the spark plug ignites the mixture and initiates the combustion which continues during the expansion stroke.

Expansion stroke:

The chemical energy in the fuel is now being converted into power, heat and emissions. The pressure increases as the expanding burning mixture drives the piston downwards and forces the crankshaft to rotate.

Exhaust stroke:

The combusted gas flows into the exhaust manifold from the cylinder due to the pressure difference and the upwards movement of the piston. As a result of this the cylinder pressure drops down to nearly the same pressure as in the exhaust manifold. When the piston reaches TDC the four stroke cycle ends and a new cycle is commenced.

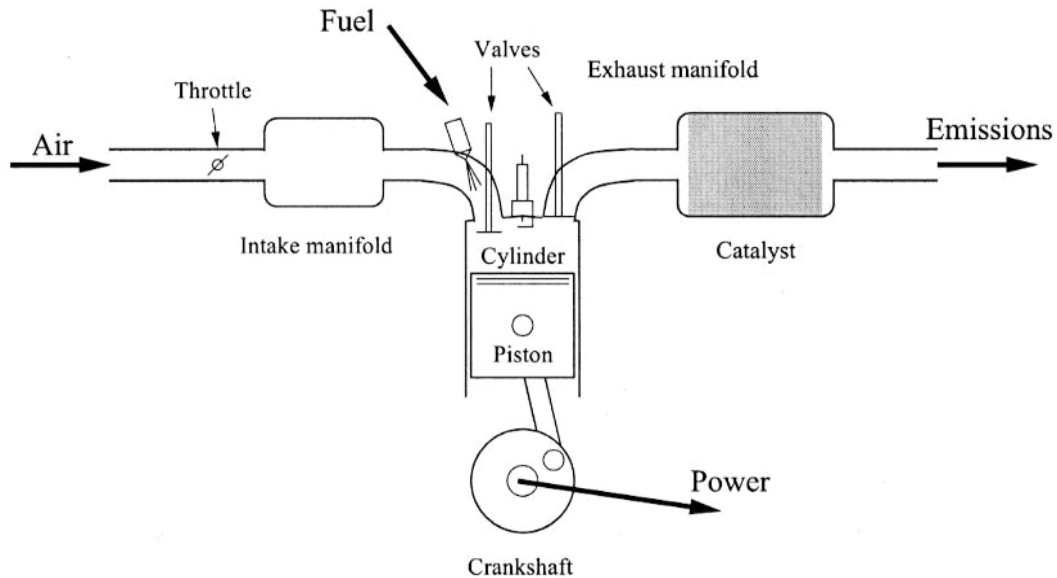


Fig 2.1: A schematic picture of a four stroke SI engine. The engine uses air and fuel to generate power, heat and emissions. The picture is taken from [1] and used with permission from the authors.

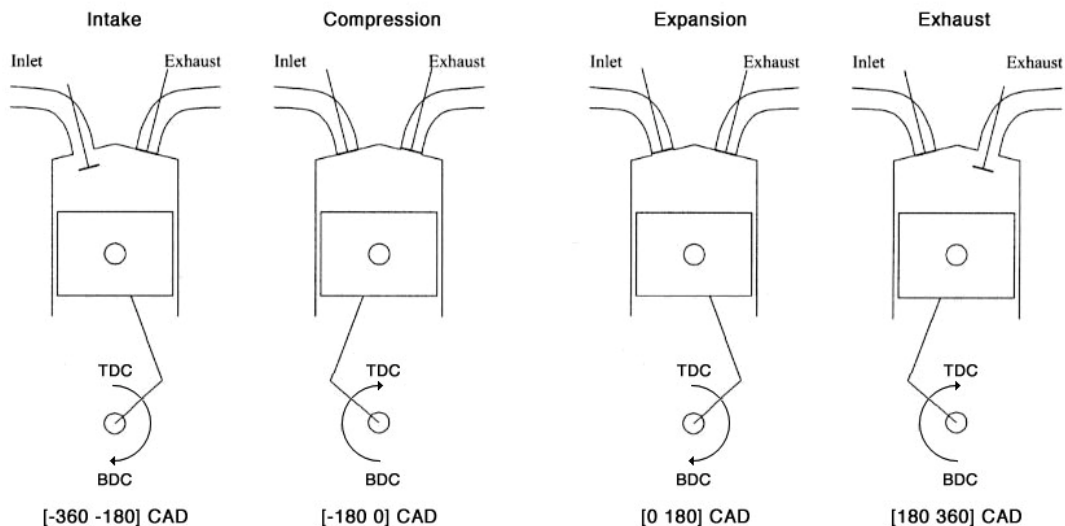


Fig 2.2: The four strokes intake, compression, expansion and exhaust of a four stroke SI engine. The picture is taken and modified from [1] and used with permission from the authors.



The variation of the cylinder pressure during the four stroke cycle plotted against the CAD is illustrated in figure 2.3. The shape and magnitude of the cylinder pressure curve and the CAD of the peak pressure position (PPP) depends on the current operating condition and when the SA occurred. The work produced by a four stroke engine during a full combustion cycle can be expressed as

$$W_{cycle} = \int_{-2\pi}^{2\pi} T(\theta)d\theta = \int_{-2\pi}^{2\pi} p(\theta)AL(\theta)d\theta \quad (2.1)$$

where  $\theta$  is the CAD,  $T$  instantaneous torque,  $p$  cylinder pressure,  $A$  cylinder cross section area and  $L$  crankshaft lever. The equation tells us that it is important to choose the right SA for a given operating condition since the work generated by the engine is integrated from the torque and the torque is generated by the cylinder pressure on the piston.

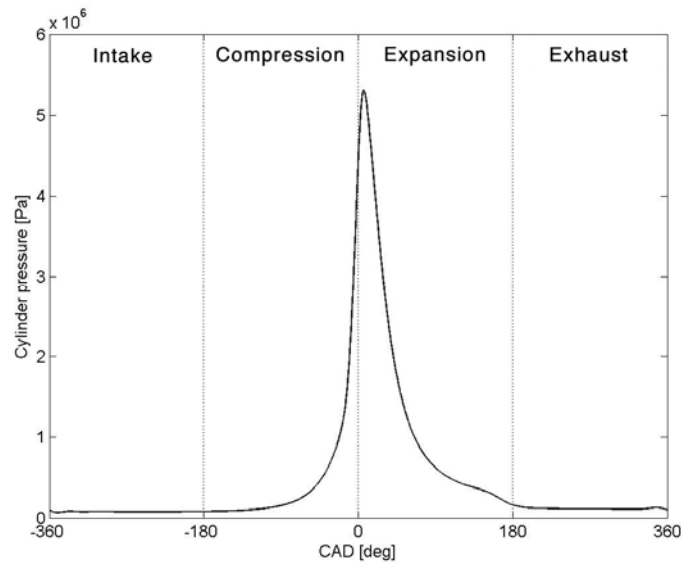


Figure 2.3: The variation of the cylinder pressure during the four stroke cycle. The different strokes are separated by dashed lines.

## 2.2 SA and MBT timing

The importance of choosing the right SA for a given operating condition can be illustrated by running the engine at a fixed operating condition while the SA is varied. A spark sweep was conducted for the SA:s -35, -30, -25, -20, -15 and -10 CAD with 250 measured combustion cycles each when the engine was operated at the engine speed  $N = 2000\text{rpm}$  and engine load  $p_{im} = 80\text{kPa}$ . Four of the SA:s used in the spark sweep are then used to illustrate the effect of SA on the cylinder pressure and the instantaneous torque from equation (2.1). From the top figure 2.4 it can be seen that an early SA results in an earlier pressure build-up and also lower pressure during the later part of the expansion stroke. A too early pressure build-up during the compression stroke counteracts the piston motion and lowers the output torque. Later SA results in a later pressure build-up which can take advantage of the greater crankshaft lever as can be seen in the middle figure 2.4. But with a too late pressure build-up the gains with a higher pressure during the later part of the expansion stroke can not compensate for the losses earlier as seen in the lower figure 2.4. Optimal SA positions the cylinder pressure in a way that compromise between the effects mentioned above and maximises the torque. This optimal SA is called maximum brake torque (MBT) timing and SA:s that are more advanced or retarded from this optimum results in a lower torque.

The SA for MBT timing is often determined by performing a spark sweep while the engine brake torque is measured. In figure 2.5 a third order polynomial estimate of the engine brake torque as a function of SA have been plotted for the whole spark sweep. The SA that would result in maximum engine brake torque is  $-21.0$  CAD.

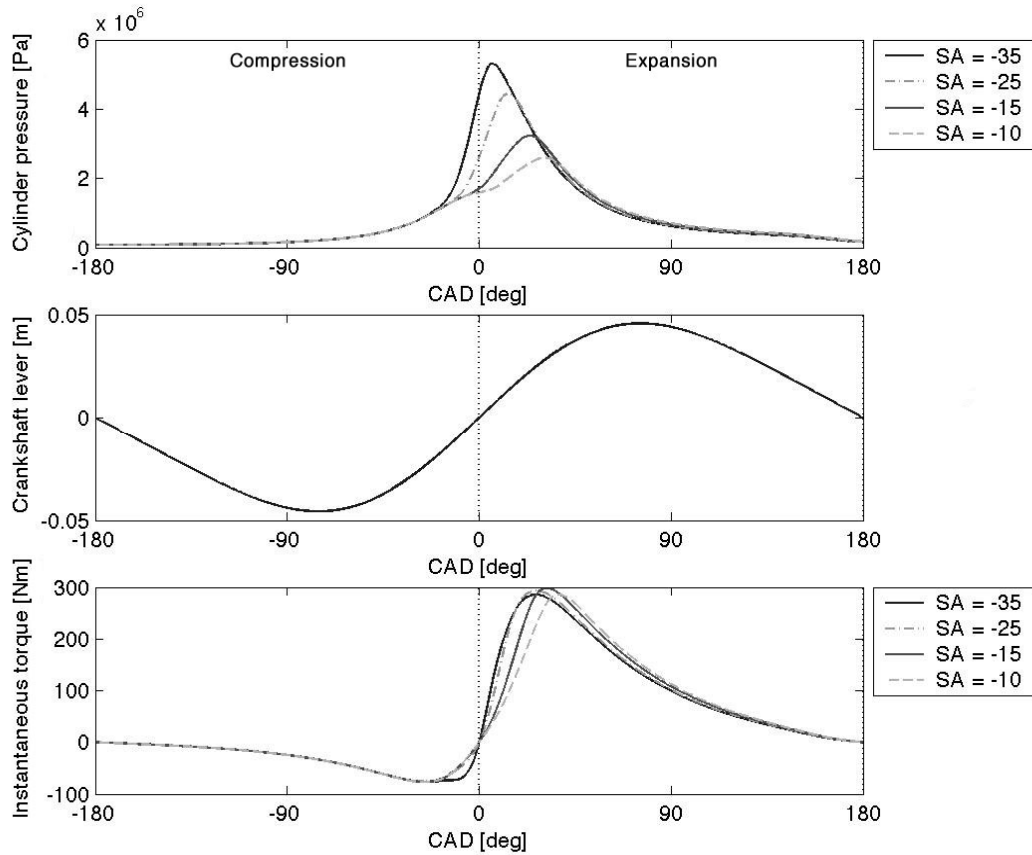


Figure 2.4: A spark sweep was conducted when the engine was operated at  $N = 2000\text{rpm}$  and  $p_{im} = 80\text{kPa}$ . Top: The cylinder pressure  $p$ . Middle: The crankshaft lever  $L$ . Bottom: The instantaneous torque  $T$  from equation (2.1).

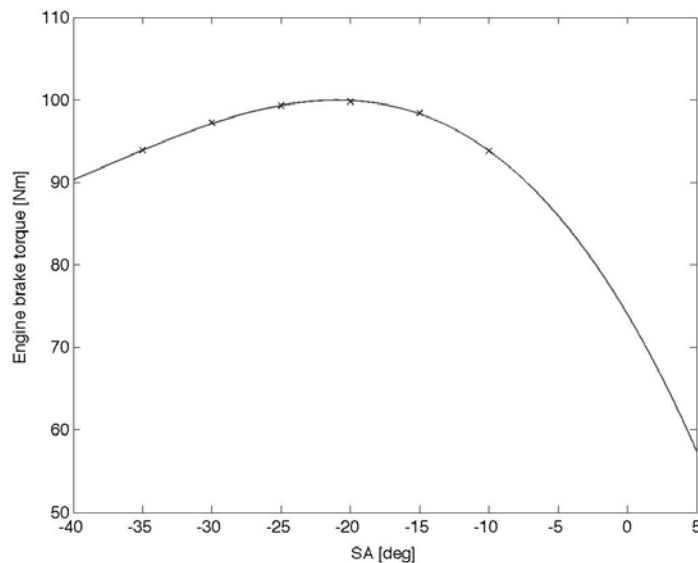


Figure 2.5: Effect of SA on engine brake torque when the engine was operated at  $N = 2000\text{rpm}$  and  $p_{im} = 80\text{kPa}$ . The SA for MBT timing is  $-21.0$  CAD.

The benefits of running an engine at MBT are several. Besides maximising the output torque, the fuel consumption is kept down to a minimum and the efficiency of the engine is maximised. In reality the optimal SA is often restricted by emission regulations and engine knock. For example at high engine loads the SA has to be retarded to prevent engine destruction by knock. The goal of this thesis is to investigate if it is possible to find the MBT timing for every operating condition. So no restriction from either knock control or emission regulation will be taken into account in this thesis.

The shape and position of the engine brake torque curves change for different operating conditions as does the SA for MBT timing. To illustrate this, 5 different spark sweeps were conducted when the engine was operated at  $N = 1200\text{rpm}$   $p_{im} = 40\text{kPa}$ ,  $2000\text{rpm}$   $70\text{kPa}$ ,  $2000\text{rpm}$   $80\text{kPa}$ ,  $3000\text{rpm}$   $50\text{kPa}$  and  $4000\text{rpm}$   $60\text{kPa}$ . For the engine operating points 6 different SA:s were used consisting of 250 measured combustion cycles except for  $2000\text{rpm}$  and  $70\text{kPa}$  where 9 different SA:s were used consisting of 100 cycles. The results are plotted in figure 2.6 as third order polynomial estimates of the averaged engine brake torque as a function of the SA. It can be observed from the figure that a higher engine load results in a greater output torque and that the curves are quite flat at the position of the maximum which means that an estimate of the MBT position does not have to be so precise.

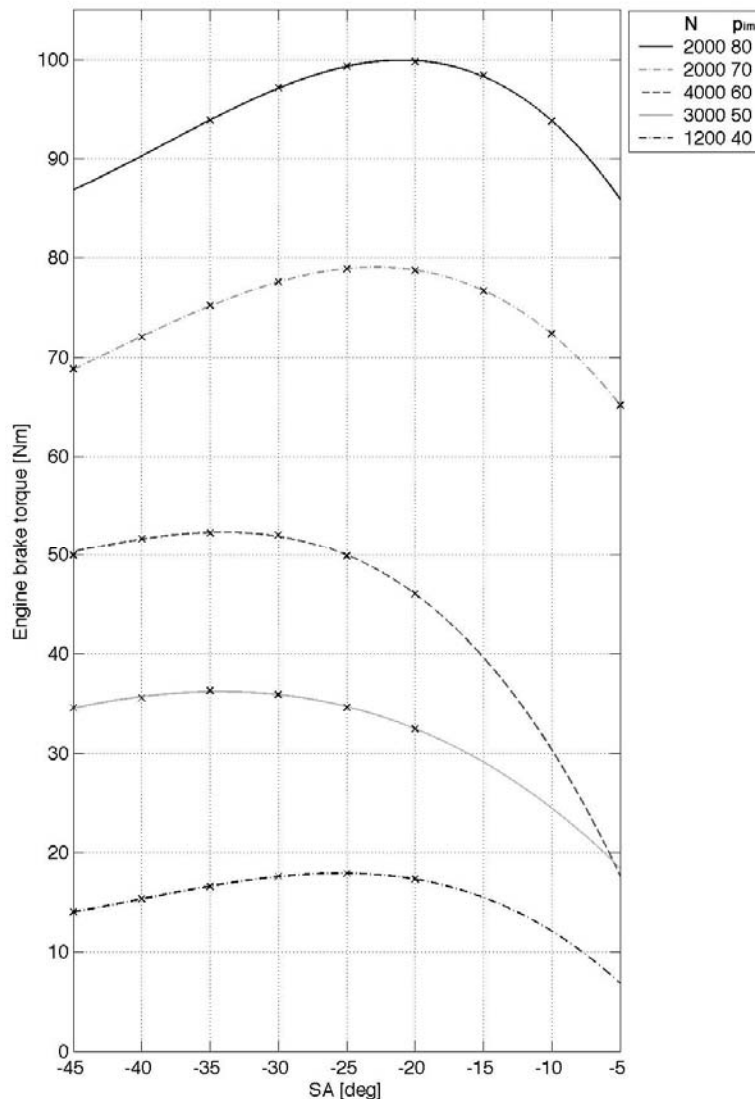


Figure 2.6: Five different spark sweeps and the corresponding third order polynomial estimates of the engine brake torque as a function of SA.

In table 2.1 the SA:s that would result in MBT timing have been calculated from the curves plotted in figure 2.6. It can be noticed that the SA for MBT timing is not constant. In fact, it depends on several parameters such as air/fuel ratio (AFR), exhaust gas recirculation (EGR), engine speed, engine load, fuel characteristics, coolant temperature, air temperature and humidity. In modern engines the SA is usually controlled by an open-loop system that uses static lookup tables and then measures several of these parameters to adjust the SA. However it is too expensive to measure and account for all the parameters that effect the SA which results in that engines are not running at their optima. A different approach is therefore to use a closed-loop system and measure the result of the SA rather than measuring all the parameters known to affect the SA.

N [rpm]	$p_{im}$ [kPa]	SA [deg]
1200	40	-25.4
2000	70	-22.9
2000	80	-21.0
3000	50	-34.2
4000	60	-34.1

Table 2.1: The SA for MBT timing is not constant for different operating conditions.

## 2.3 Combustion descriptors

From data observations several empirical rules that relate variables called combustion descriptors [2] from the cylinder pressure to the optimal SA have been derived. The combustion descriptors describe how the combustion develops in relation to the CAD and are therefore suitable for closed-loop control of the SA for MBT timing. This thesis will focus on the combustion descriptors called PPP, 50%MFB and MAMFB.

### 2.3.1 PPP

The peak pressure position (PPP) is the CAD where the cylinder pressure reaches its maximum value

$$\theta_{PPP} = \arg \max_{\theta} (p(\theta)) \quad (2.2)$$

where  $\theta$  is the CAD and  $p$  the cylinder pressure. It has been shown by [3, 4] that for MBT timing the position of the PPP is fairly constant around 16 CAD after top dead center (ATDC) regardless of the engine's operating condition. In [5] the PPP is claimed to be around 15 CAD ATDC and according to [1] the PPP varies between 12-20 CAD ATDC depending on engine design but is fairly constant for a given engine.

### 2.3.2 50%MFB

Another possibility for describing the combustion development is to use the mass fraction burned (MFB). The MFB describes how the combustion process consumes fuel in relation to the CAD and is calculated using the measured cylinder pressure and the cylinder volume. The MFB can be obtained through various models for example Rassweiler-Withrow [6], apparent heat release [7], Matekunas pressure ratio [8] and Gatowski et al [9]. In [10] the mentioned models are described, implemented and evaluated. The model used for calculating the MFB in this thesis is the Rassweiler-Withrow method because of its simplicity to implement and it being computationally efficient. In the Rassweiler-Withrow model described in [10] the actual

pressure change  $\Delta p = p_{j+1} - p_j$  during the interval  $\Delta\theta = \theta_{j+1} - \theta_j$ , where the CAD  $\theta$  at each sample  $j$  is known, is assumed to be made up of a pressure rise due to combustion  $\Delta p_c$  and a pressure rise due to volume change  $\Delta p_v$ .

$$\Delta p = \Delta p_c + \Delta p_v \quad (2.3)$$

The pressure change due to volume change  $\Delta p_v$  during the interval  $\Delta\theta$  is given by the polytropic relation

$$pV^n = \text{constant} \quad (2.4)$$

where  $p$  is the cylinder pressure,  $V$  the cylinder volume and  $n$  the polytropic index. According to [11] a polytropic index in the interval [1.25 1.35] have shown to give a good fit to experimental data. Here the averaged index  $n = 1.3158$  from [3, page 178] is used. With the help of (2.4) the rise due to the volume change  $\Delta p_v$  can be expressed as:

$$\begin{aligned} \Delta p_v(j) &= p_{j+1,v} - p_{j,v} = \\ &= \left[ p_{j,v} V_j^n = p_{j+1,v} V_{j+1}^n \Leftrightarrow p_{j+1,v} = p_{j,v} \left( \frac{V_j}{V_{j+1}} \right)^n \right] = \\ &= p_{j,v} \left( \left( \frac{V_j}{V_{j+1}} \right)^n - 1 \right) \end{aligned} \quad (2.5)$$

Applying (2.3), (2.5) and  $\Delta p = p_{j+1} - p_j$  yields the pressure change due to the combustion as

$$\Delta p_c(j) = p_{j+1} - p_j \left( \frac{V_j}{V_{j+1}} \right)^n \quad (2.6)$$

By assuming that the pressure rise due to combustion in the interval  $\Delta\theta$  is proportional to the mass of mixture that burns, the MFB at the end of the  $j$ 'th interval thus becomes

$$x_b(j) = \frac{m_b(j)}{m_b(\text{total})} = \frac{\sum_{k=0}^j \Delta p_c(k)}{\sum_{k=0}^M \Delta p_c(k)} \quad (2.7)$$

Where  $M$  is the total number of crank angle intervals and  $\Delta p_c(k)$  is found from (2.6). In [12] using either 45% or 50% of the MFB is suggested as a combustion descriptor. The combustion descriptor chosen in this thesis is the 50%MFB because it is the most commonly used and therefore it is easier to compare the conclusions in this thesis with the results of previous works.

$$\theta_{50\%MFB} = \arg(x_b(\theta_j) = 0.5) \quad (2.8)$$

where  $\theta$  is the CAD and  $x_b(\theta_j)$  the MFB. When using 50%MFB as a combustion descriptor the MBT timing occurs at about 10 CAD ATDC according to [3] which has been further investigated and confirmed by [13]. In [5] the 50%MFB position for MBT timing is claimed to be around 8-10 CAD ATDC.

### 2.3.3 MAMFB

In [14] a combustion descriptor called Maximum Acceleration of Mass Fraction Burned (MAMFB) is introduced. It is the maximum point of the second derivate of the MFB

$$\theta_{MAMFB} = \arg \max_{\theta} \left( \frac{\partial^2 x_b(\theta_j)}{\partial \theta^2} \right) \quad (2.9)$$

where  $\theta$  is the CAD and  $x_b(\theta_j)$  the MFB from (2.7). According to the authors the MBT timing occurs when the MAMFB point is located at 0 CAD. However, it is also mentioned that this hypothesis needs to be validated with the help of extensive test data.

### 2.3.4 Illustrated examples

The different curves used for calculating the combustion descriptors  $\theta_{PPP}$ ,  $\theta_{50\%MFB}$  and  $\theta_{MAMFB}$  are illustrated in figure 2.7 for the earlier performed spark sweep at  $N = 2000\text{rpm}$  and  $p_{im} = 80\text{kPa}$  plotted in figure 2.6. The cylinder pressure is used to calculate the  $\theta_{PPP}$ , while the  $\theta_{50\%MFB}$  is calculated from the MFB and the AMFB is used to calculate the  $\theta_{MAMFB}$ .

The different values of the combustion descriptors for MBT timing are then calculated for all of the spark sweeps plotted in figure 2.6 and the result can be studied in table 2.2. The SA:s for MBT timing was taken from table 2.1 and a linear interpolation was used to extract the corresponding values of the combustion descriptors for those SA:s. From the table it can be observed that during the different spark sweeps the variation of the SA for MBT timing is 13.3 CAD while the combustion descriptors are fairly constant with a variation of only 2.1-3.3 CAD.

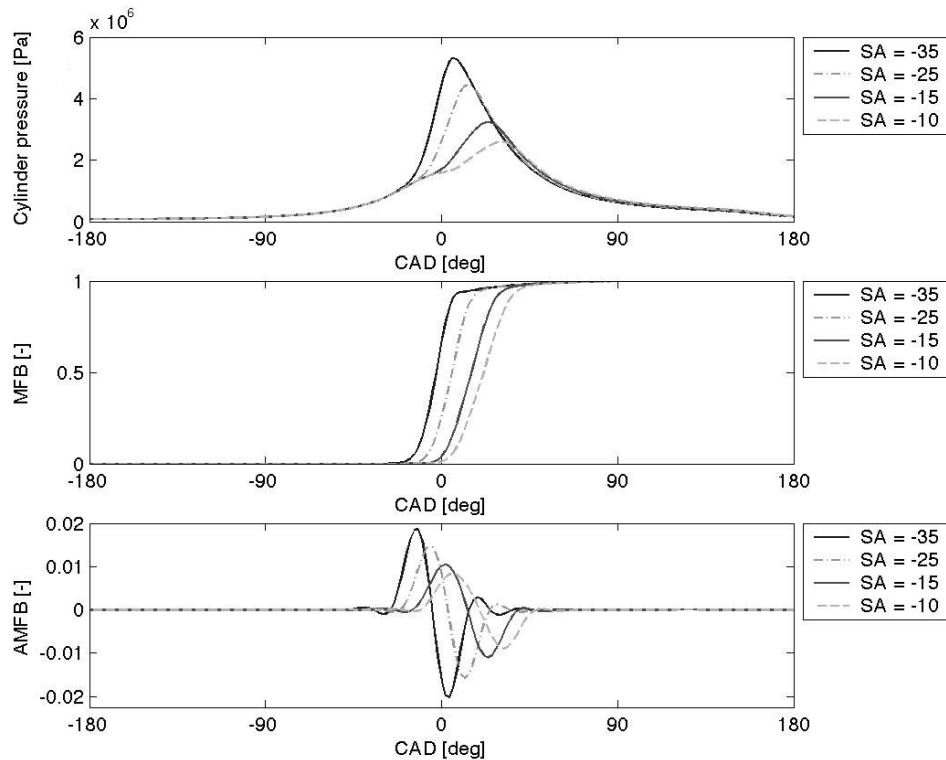


Figure 2.7: The different curves used for calculating the combustion descriptors  $\theta_{PPP}$ ,  $\theta_{50\%MFB}$  and  $\theta_{MAMFB}$  for the earlier performed spark sweep at  $N = 2000\text{rpm}$  and  $p_{im} = 80\text{kPa}$  plotted in figure 2.6. Top: The cylinder pressure. Middle: The mass fraction burned (MFB). Bottom: The acceleration of mass fraction burned (AMFB).

N [rpm]	$p_{im}$ [kPa]	SA [deg]	$\theta_{PPP}$ [deg]	$\theta_{50\%MFB}$ [deg]	$\theta_{MAMFB}$ [deg]
1200	40	-25.4	17.3	8.6	-4.2
2000	70	-22.9	16.6	8.1	-4.3
2000	80	-21.0	17.4	9.0	-3.6
3000	50	-34.3	15.9	7.6	-5.7
4000	60	-34.1	14.3	5.7	-5.6
Variation:		13.3	3.1	3.3	2.1

Table 2.2: The different SA:s and combustion descriptors values for MBT timing for the spark sweeps plotted in figure 2.6. The variation of SA for MBT timing is 13.3 CAD while the combustion descriptors are fairly constant with a variation of 2.1-3.3 CAD.

## 2.4 %MBT performance

To be able to evaluate the performance of a closed-loop control of the SA for MBT timing system, one must be able to tell how much loss of torque a SA error in CAD from the MBT position corresponds to. By dividing each of the torque curves plotted in figure 2.6 with their maximum value and then aligning them so that the maximum positions are at 0 CAD, curves which describe how many percent of MBT (%MBT) a SA error in CAD from the MBT position corresponds to are attained. The SA error is calculated with

$$\theta_{error} = \theta - \theta_{MBT} \quad (2.10)$$

where  $\theta$  is the used SA and  $\theta_{MBT}$  is the SA for MBT timing. In figure 2.8 it can clearly be seen that the impact of an error on the output torque depends on which operating condition the engine is running at. Since only 5 spark sweeps at different operating conditions were

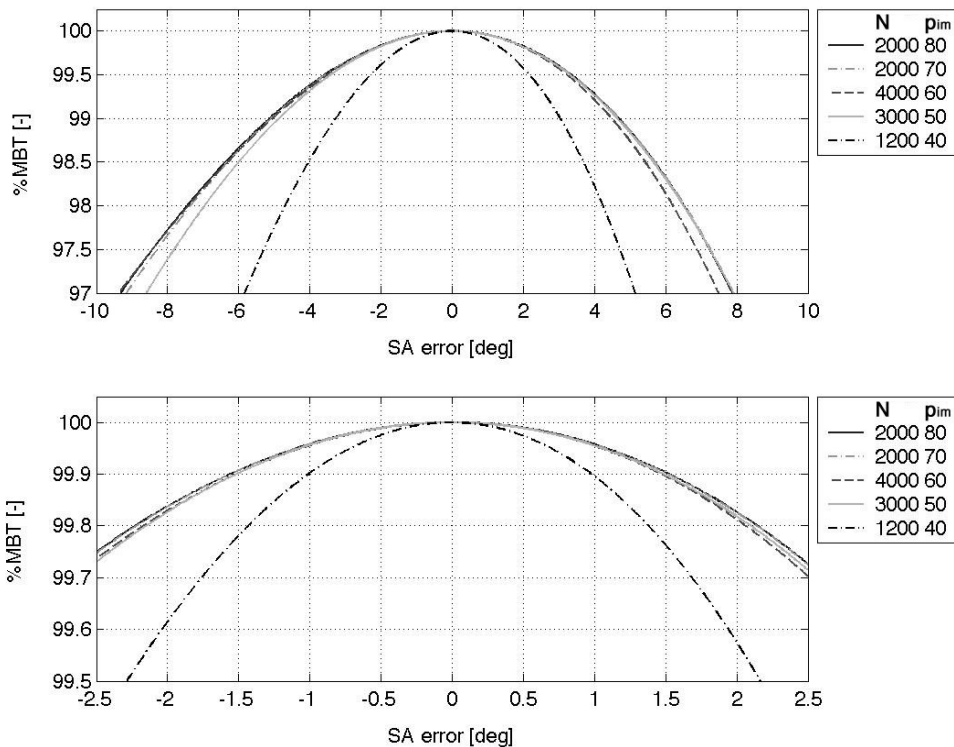


Figure 2.8: Different zooms of how many percent of MBT a SA error in CAD from the MBT position corresponds to for different operating conditions.

measured, no thorough investigation was able to be made. But the measurements give a hint of how much %MBT a CAD error from the MBT position corresponds to. As mentioned earlier the SA is often retarded to avoid knock and the most interesting part of the curves is therefore for positive CAD errors. The greatest sensitivity against a SA error with the given data is when the engine is running at  $N = 1200\text{rpm}$  and  $p_{im} = 40\text{kPa}$ . For this operating condition a SA error of for example +2 CAD from the MBT position results in an output torque corresponding to 99.58% of MBT.

Another way of evaluating the performance of a closed-loop control of the SA for MBT system is to study how an error in the result of the SA affects the engine brake torque. The same spark sweeps as for figure 2.6 were used but instead of estimating third order polynomials of the engine brake torque as a function of the SA, the engine brake torque was made dependant of the combustion descriptor PPP. For a given operating point and SA value, the cylinder pressure is used to calculate the PPP which then is used to estimate a third order polynomial of the engine brake torque as a function of the PPP. The reasons for only investigating the combustion descriptor PPP are that the PPP is easy to calculate directly from the cylinder pressure with a high accuracy and no modelling is needed as for the combustion descriptors 50%MFB and MAMFB. To do the same thing for the other combustion descriptors a better MFB model than the Rassweiler-Withrow would have to be used. The  $\theta_{\text{error}}$  was calculated on the same way as in equation (2.10) with the difference that the PPP was used instead of the SA. The result can be studied in figure 2.9 where it can be seen that a low engine load results in a greater sensitivity against a PPP error in terms of %MBT. The explanation for this is that the total cylinder pressure is a sum of two pressure curves; the motored pressure resulting from the cylinder's volume change and the pressure from the combustion process. When the engine load is low the motored pressure has a greater influence on the total cylinder pressure which makes it more important to align the two pressure curves so that maximum torque is attained. As the engine load increases, the pressure from the

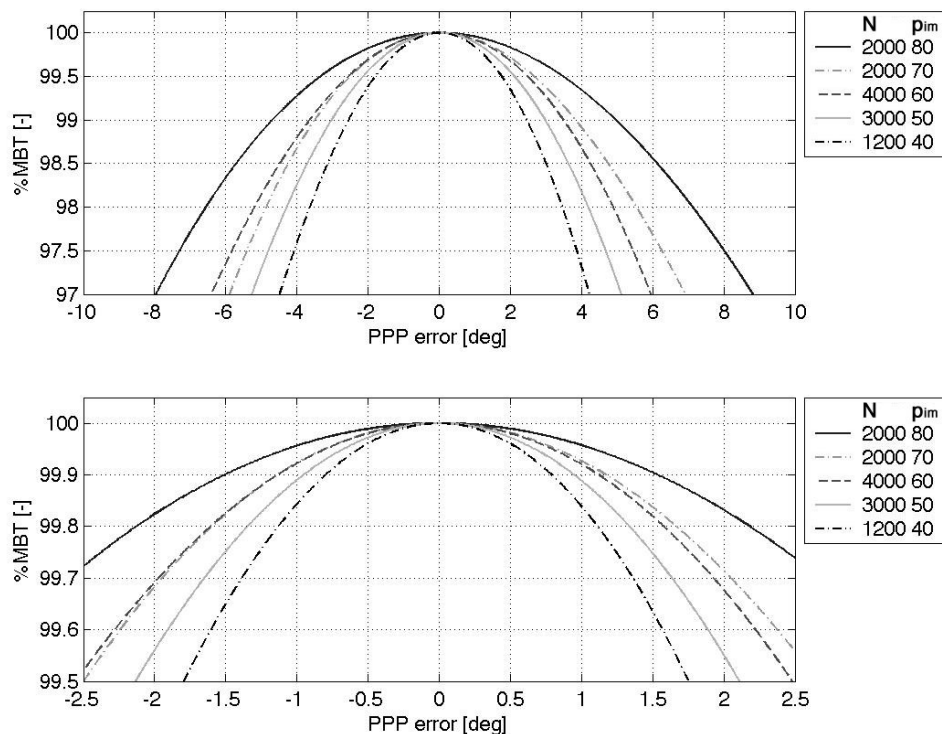


Figure 2.9: Different zooms of how many percent of MBT a PPP error in CAD from the MBT position corresponds to for different operating conditions.



combustion process increases resulting in a greater influence on the PPP which makes the engine brake torque less sensitive against an error in the PPP.

The most desirable would be to estimate the combustion descriptors directly from a cylinder pressure sensor. But due to their high cost and the added complexity for design and manufacturing they are not conceivable for mass production yet. The most economic and therefore most realistic alternative is to use the already existing spark plug to estimate the descriptors from the ionization current measurements. Several publications have shown a high correlation between the combustion descriptors estimated from the cylinder pressure and ionization current which is promising for closed-loop control of the MBT timing [5, 15, 16, 17].



## Chapter 3

### The ionization current

The combustion descriptors estimated from the cylinder pressure presented in section 2.3 can be used for closed-loop control of the SA for MBT timing. Since cylinder pressure sensors are too expensive, the alternative is to use the ionization current measured by the already existing spark plug. The ionization current contains information about the cylinder pressure but is also affected by several other parameters in a complex way.

First the ionization current is explained from a MBT perspective. Then the influence of fuel additives and the engine operating parameters  $\lambda$ , EGR, engine load, engine speed and SA on the amplitude and phasing of the ionization current are investigated for two inductive ignition systems with different ignition durations.

#### 3.1 Origin and measurement

The combustion in a SI engine is normally initiated with a spark discharge from the spark plug during the compression stroke. A flame develops and travels from the location of the spark plug to the cylinder walls as it consumes the air-fuel mixture contained in the cylinder. The chemical reactions in the flame front and the raised temperature create free ions through various ionization processes. By applying a DC bias to the spark plug after the spark has vanished an electrical field is generated. The electrical field forces the ions to move which generates an ionization current. The sensed current depends on the ions created, on their relative concentration and recombination rate, on pressure and on temperature to mention some of the most important factors. The processes behind the creation of the ions during the combustion have been investigated but their relative importance as contributors to the current is not yet fully understood.

#### 3.2 Cycle-to-cycle variations

The ionization current has a characteristic shape as can be seen in the top figure 3.1. The ionization current is often illustrated using an average of several consecutive cycles that have been sampled during constant external conditions. It is therefore very unlikely to encounter an

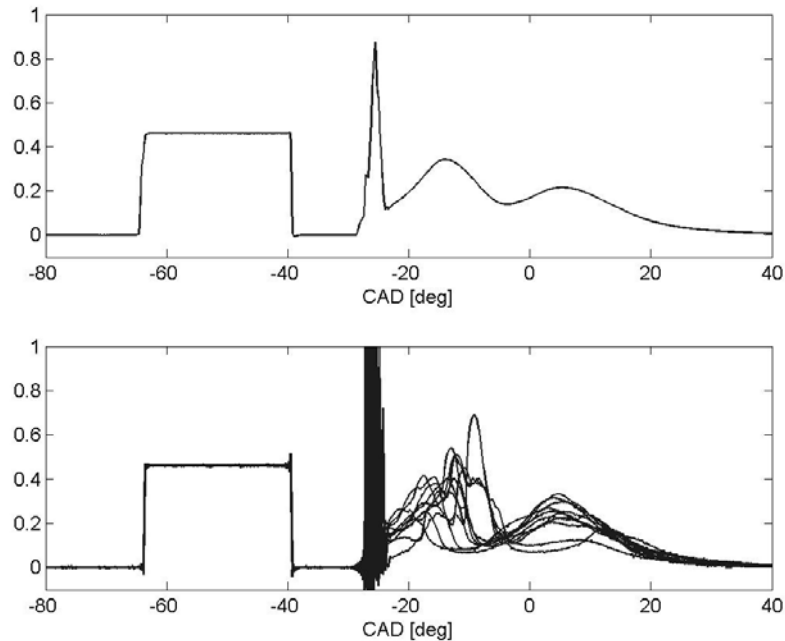


Figure 3.1: The engine was operated at steady state for  $N = 1200\text{rpm}$ ,  $p_{im} = 40\text{kPa}$  and  $SA = -40\text{CAD}$ . Top: The ionization current is averaged over 250 cycles. Bottom: The always present cycle-to-cycle variations are illustrated by plotting 10 consecutive measured cycles.

example like the one plotted in the top figure 3.1 since large combustion variations from one cycle to another always are present in SI engines. These variations must be taken into consideration since they put a constraint on the engines performance. The bottom figure 3.1 shows 10 consecutive measured ionization curves when the engine was operated at steady state condition that clearly shows the unpredictable cycle-to-cycle variations. In [3] three causes for the variations are explained:

- The motion of the air-fuel mixture contained in the cylinder varies from one combustion cycle to another.
- The amount of released energy is affected by the variations in the amount of fuel, air and recycled gases contained in the cylinder.
- There is one spatial distribution of fuel, air and recycled gases for one combustion cycle and another spatial distribution for the next. The spatial distribution nearest the spark plug is important for the early development and propagation of the flame front which affects the cycle-to-cycle variations.

The cycle-to-cycle variations influence on MBT timing have been investigated in [12] where the conclusion was drawn that the variations only have a minor influence on the optimal SA and can be neglected when considering closed-loop control of SA for MBT timing.

### 3.3 The three phases

The ionization current is often divided into three parts which reflect the different stages of the combustion development; the ignition phase, the flame front phase and the post flame phase which are illustrated in figure 3.2. Each of these phases has varying characteristics and they also tend to overlap in complicated ways.

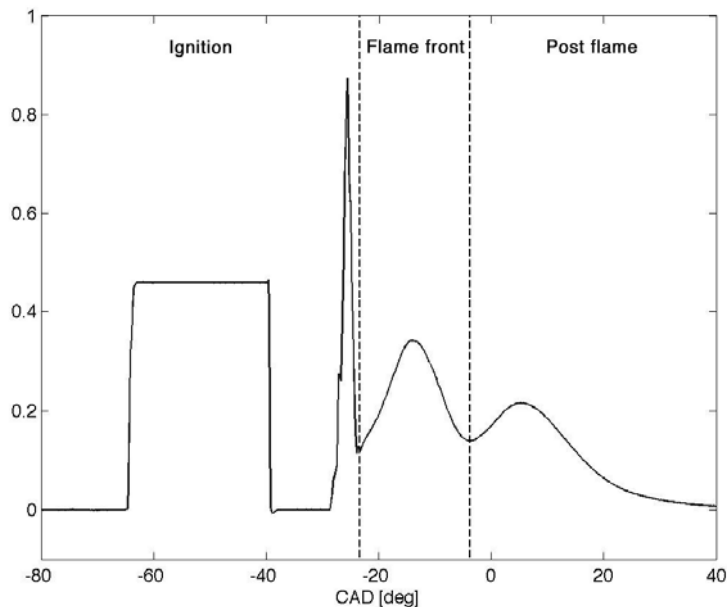


Figure 3.2: The three phases of the averaged ionization current; the ignition phase, the flame front phase and the post flame phase separated by dashed lines.

### 3.3.1 Ignition phase

The first part of the ionization current is called the ignition phase. During this phase the air-fuel mixture contained in the cylinder is ignited by the ignition system. The two different ignition systems used here are of inductive discharge type with different ignition durations. The type of system used will affect the shape of the ionization current during the ignition phase as can be seen in figure 3.3.

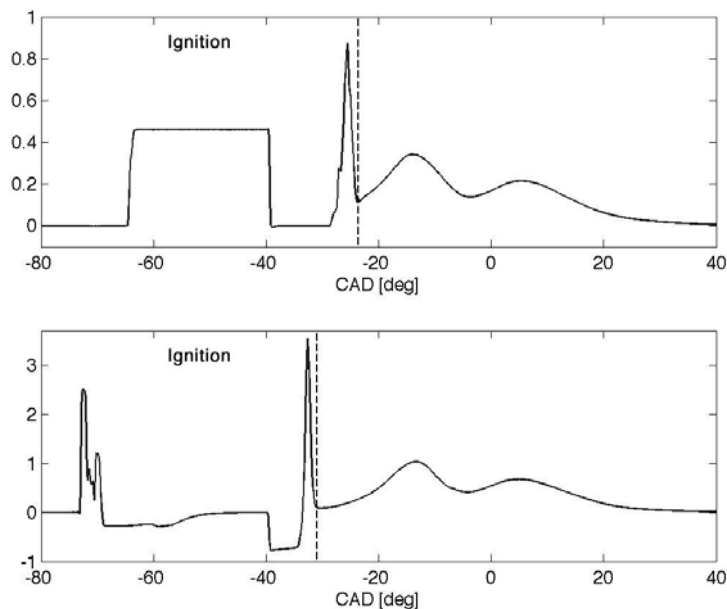


Figure 3.3: The differences in the ignition phase when using an ignition system with a short or a long ignition duration. Top: The averaged ionization current when using the ignition system in cylinder 2 with a long ignition duration. Bottom: The averaged ionization current when using the ignition system in cylinder 1 with a short ignition duration.

The first part of the ignition phase is the charging of the coil. When the coil is powered up it will stay so until it discharges at the desired ignition angle which causes the ionization curve to rapidly drop down. After the ignition the ringing phenomenon can be seen. The phenomenon originates from the quick spark discharge and the remaining electrical charges in the circuits. The length of the ringing phenomenon mainly depends on the speed of the engine at the current operating point and the dwell time which is the charge time of the coil used in the ignition system. A greater engine speed or longer dwell time result in a more violent and prolonged ringing phenomenon. Since no information about the combustion process is incorporated in the ringings they are often removed to simplify for further signal interpretation.

### **3.3.2 Flame front phase**

During the flame front phase a flame develops and ions are believed to be formed due to various chemical ionization processes in the reaction zone of the propagating flame [18]. The exact beginning of the flame front phase is often hard to determine due to the overlap with the ringing phenomenon from the ignition phase. If the overlap is too wide some of the combustion information in the beginning of the flame front phase can be destroyed.

The ions generated by the chemical ionization have different recombination rates. Some ions recombine very quickly to more stable molecules while others last longer due to longer residual times. This results in one or more characteristic peaks which declines as more and more ions recombine to molecules. The ionization current during the flame front phase has shown to be well correlated with the MFB [17] and the air/fuel ratio (AFR) [18, 19].

### **3.3.3 Post flame phase**

In the last phase of the ionization current the most stable ions remain and the combustion temperature often increases to such a degree that new ions are formed through thermal ionization. After the decline of the ionization curve during the end of the flame front phase, the curve now starts to build up again and form a peak known as the thermal peak. The thermal peak is from empirical observations known to have a strong correlation with the PPP [15, 16]. It has been investigated and confirmed in [15, 18] that the thermal ionization of nitrogen monoxide (NO) is the main contributor of free ions in the combustion chamber during high temperatures. The NO ions are formed in the high temperature burned gases behind the flame front. A higher temperature results in a higher rate of NO formation. Even though more dominating species like CO<sub>2</sub>, H<sub>2</sub>O and N<sub>2</sub> exist in the combustion gas, they all have so much higher ionization energy that the total number of ionized particles from these three is much less than from NO. For lower temperatures where not enough NO ions are formed, the alkali metals such as Potassium (K) and Sodium (Na) are suspected to play an important role for the occurrence of the thermal peak [20, 21, 22].

The thermal peak may also disappear as seen in figure 3.4 for approximate 10-20 CAD if the temperature of the burned gases does not reach the ionization temperature threshold. The probability for this to happen increases when the engine is operated with a combination of the following engine parameter settings which lowers the combustion temperature and therefore the rate of NO formation; a very low or high  $\lambda$ , a high EGR rate, low engine load, low engine speed or late SA. This conclusion is reached in the next section where an investigation of how the shape of the ionization current is altered when changing one of the engine operating parameters mentioned above at a time.

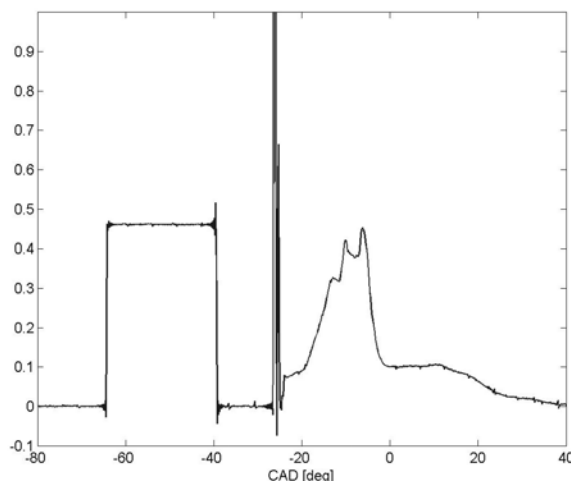


Figure 3.4: A minor thermal ionization for  $N = 1200\text{rpm}$ ,  $p_{im} = 40\text{kPa}$  and  $SA = -40\text{ CAD}$ .

### 3.4 Influence of engine operating parameters

An investigation has been made how the amplitude and phasing of the flame front and post flame phases of the ionization current are affected by changes in the engine operating parameters  $\lambda$ , EGR, engine load, engine speed and SA. The parameters sweeps in table 3.1 were made while the engine was operated under the conditions described in table 3.2. For each measuring point 100 combustion cycles were measured and the cylinder pressure and ionization curves were averaged. Both 2D and 3D figures have been plotted for each sweep to be able to study the visible effects on the shape of the ionization curve. The focus is on interpreting the visible effects and later being able to test the robustness of the algorithms used for estimating the combustion descriptors mentioned in section 2.3.

$\lambda$	0.77 0.88 0.98 1.09 1.2 [-]
EGR overlap	28 32 38 42 47 52 56 [deg]
Engine load	40 50 60 70 80 90 100 110 [kPa]
Engine speed	1200 1500 2000 2500 3000 3500 4000 [rpm]
SA	-45 -40 -35 -30 -25 -20 -15 -10 -5 [deg]

Table 3.1: The performed sweeps of the engine operating parameters.

$\lambda$	1 [-]
EGR overlap	28 [deg] - Default L850 setting
Engine load	70 [kPa]
Engine speed	2000 [rpm]
SA	Determined by the ECU

Table 3.2: The sweeps in table 3.1 were performed while the engine was operated under these operating conditions.

A summary of the investigation can be seen in table 3.3. During the engine load and engine sweep the SA was changed by the electronic control unit (ECU) which makes the measurements dependant of two engine operating parameters at a time. An example of how the table should be read is when the SA is increased during the sweep from -45 to -5 CAD, the amplitude of the flame front and post flame phase decreases and the phasing of the ionization current is shifted to the right.

	$\lambda$	EGR	Engine load (and SA)	Engine speed (and SA)	SA
Amplitude of the flame front phase	Max for $\lambda = 0.88$	↓	↑	↑	↓
Amplitude of the post flame phase	Max for $\lambda = 0.88$	↓	↑	↑	↓
Phasing of the ionization current	Unaffected	Unaffected	←	→	→

*Table 3.3: A summary of how the amplitude and phasing of the flame front and the post flame phases of the ionization current are affected when the engine operating parameters are increased one at a time..*

### 3.4.1 $\lambda$

The air/fuel ratio (AFR) is defined as the mass ratio between the air  $m_a$  and the fuel  $m_f$  in the mixture injected into the cylinder.

$$AFR = \frac{m_a}{m_f} \quad (3.1)$$

For optimal combustion efficiency the mixture should be at stoichiometric ratio when there is just enough oxygen for the conversion of all the fuel into completely oxidized products. Since the stoichiometric mixture  $AFR_s$  depends on the relative contents of hydrogen and carbon in the fuel, the AFR is therefore usually given normalized with the  $AFR_s$  and is called the relative air/fuel ratio or the air/fuel equivalence ratio.

$$\lambda = \frac{AFR}{AFR_s} \quad (3.2)$$

The  $\lambda$  parameter can directly be influenced by the throttle and fuel injection and is thus very useful for engine control. In modern vehicles equipped with three way catalysts both good emission reductions and good driveability is attained if  $\lambda$  is controlled to a narrow band around stoichiometric conditions  $\lambda = 1$ .

The following sweep of the  $\lambda$  parameter was performed:

0.77 0.88 0.98 1.09 1.2 [-]

The averaged measured ionization and cylinder pressure curves are plotted in figure 3.5. The first striking differences between the ionization currents measured in cylinder 1 and cylinder 2 are that the peak in the flame front phase has vanished for the ionization current measured in cylinder 2. This proves to be the case for all of the different engine parameter sweeps and it is a result of using of a longer dwell time in the ignition system which results in a prolonged ringing phenomenon. It can also be observed that the amplitude of the averaged ionization current measured in cylinder 2 is almost 3 times smaller than the amplitude of the current measured in cylinder 1. When studying the impact of the  $\lambda$  sweep both the ionization curves reveal similar changes in the amplitude and no change in the phasing of the ionization current when the  $\lambda$  parameter is changed. Both curves have an amplitude maximum at  $\lambda = 0.88$  which is in agreement with the results  $\lambda = 0.85$  in [20] and  $\lambda \leq 0.9$  in [18]. The amplitude decreases



when using a higher or lower  $\lambda$  value which further can be studied in the figure 3.6. The behaviour of the thermal peak in the post flame phase can be explained by looking at how the rate of NO formation changes when varying  $\lambda$ . In [3, page 582 fig 11-9] the rate of NO formation is almost formed as a second degree polynomial and has its maximum around  $\lambda = 0.9$  which is close to the found amplitude maximums of the ionization currents. This confirms that the post flame peak strongly depends on the rate of NO formation.

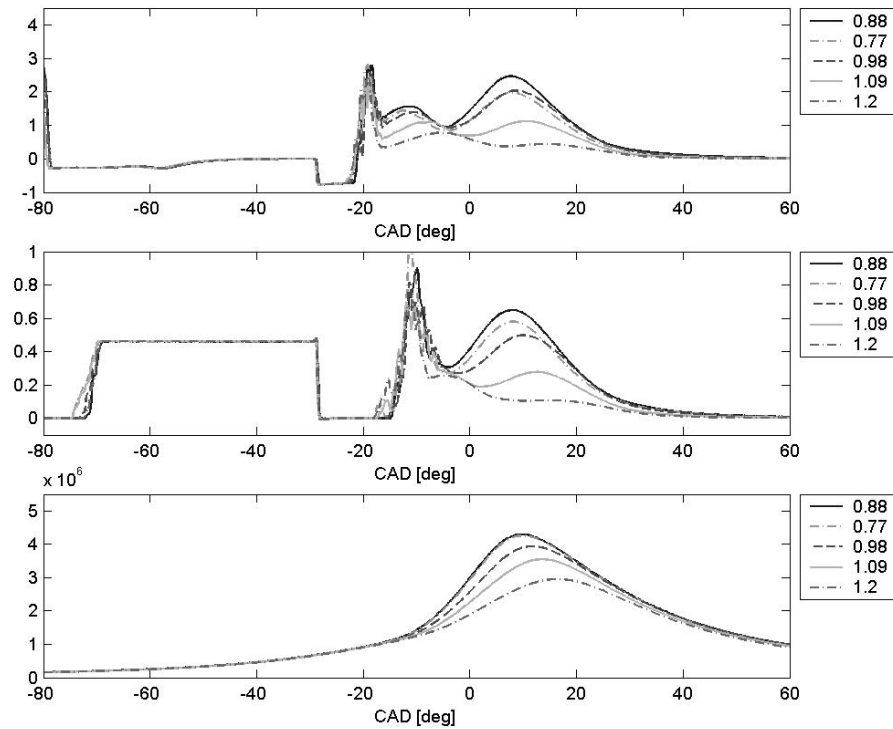


Figure 3.5: A  $\lambda$  sweep was performed while the engine was operated under the conditions described in table 3.2. Top: The averaged ionization curve measured in cylinder 1. Middle: The averaged ionization curve measured in cylinder 2. Bottom: The averaged cylinder pressure measured in cylinder 2.

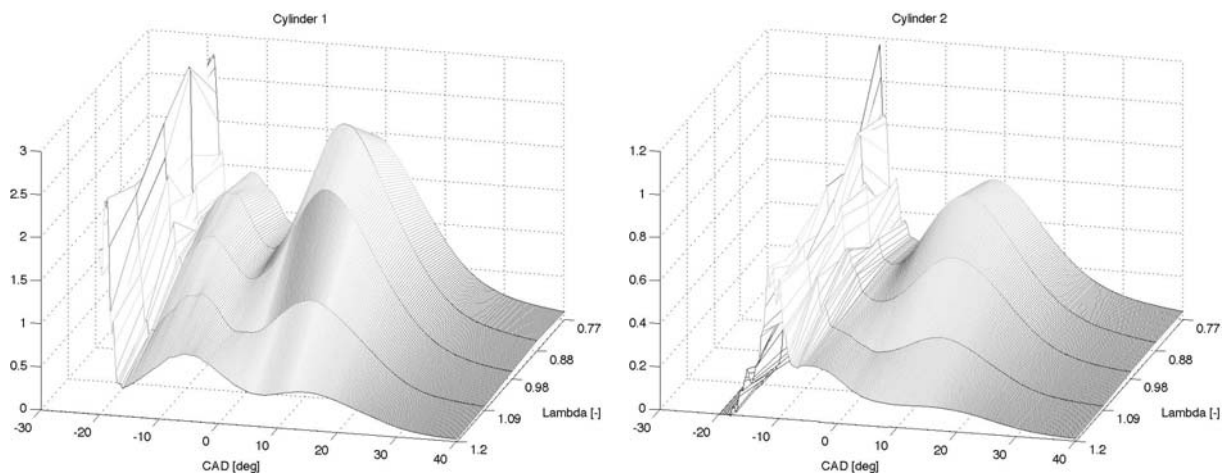


Figure 3.6: 3D plots of the averaged ionization curves measured in cylinder 1 and cylinder 2 for the  $\lambda$  sweep.

### 3.4.2 EGR

Exhaust gas recirculation (EGR) is a common technique used in modern cars for reducing  $\text{NO}_x$  emissions and lowering the fuel consumption. Most of the EGR systems today use external EGR where a portion of the burned gases are extracted from the exhaust system, returned to the intake system and mixed with the fresh air-fuel mixture. Other EGR systems like the one used in this thesis is based on a variable internal EGR which are realised by using variable valve timing. For those systems the amount of recycled gases is determined by the overlap of the exhaust maximum opening position (eMOP) and intake maximum opening position (iMOP) of the cylinder valves. A greater overlap results in more recycled gases. The presence of the already burned exhaust gases in the combustion chamber results in a lower combustion temperature and a slower combustion speed. There exists an upper limit for how much EGR the engine tolerates before HC emissions and fuel consumption is increased in combination with rougher engine operation by increased cycle-to-cycle variations and misfire.

The following sweep of the EGR parameter was performed by changing the overlap:

28      32      38      42      47      52      56      [deg]

The overlap was calculated by using the equation

$$\text{overlap} = (\text{eMOP} + 120) - (\text{iMOP} - 120) \quad (3.3)$$

and the following settings for eMOP and iMOP:

[252 464] [252 460] [252 454] [252 450] [252 445] [252 440] [252 436] [eMOP iMOP]

The results of the EGR overlap sweep can be seen in the figures 3.7 and 3.8. As expected the

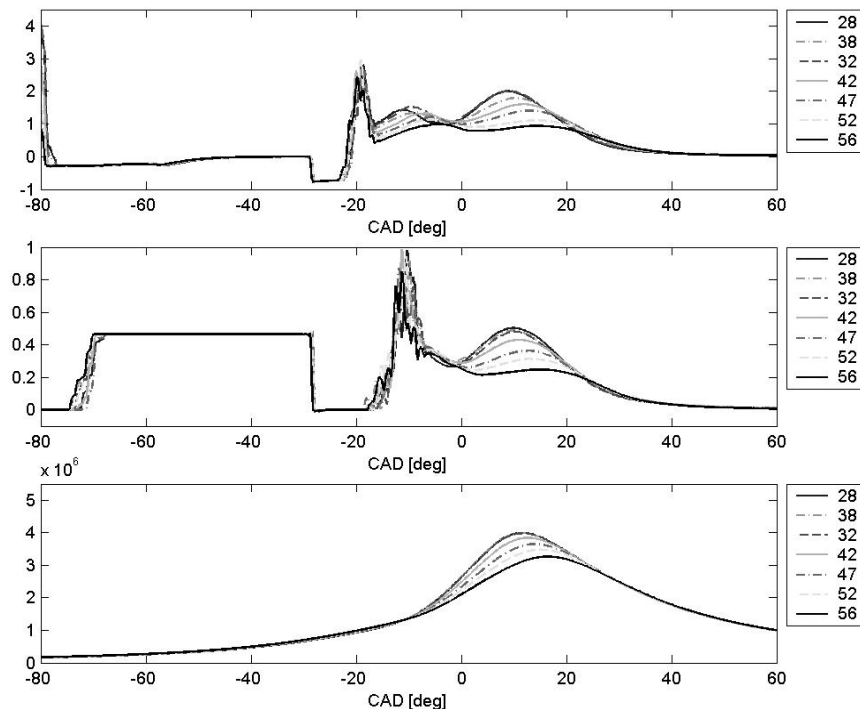


Figure 3.7: An EGR sweep was performed while the engine was operated under the conditions described in table 3.2. Top: The averaged ionization curve measured in cylinder 1. Middle: The averaged ionization curve measured in cylinder 2. Bottom: The averaged cylinder pressure measured in cylinder 2.

smallest overlap with 28° results in the highest amplitude due to less burned gases being recycled which leads to a higher combustion temperature. When the overlap increases, the amplitude of the averaged cylinder pressure and the averaged ionization curves decrease as a result of more recycled gases being present in the cylinder. This results in a lower combustion temperature, a slower combustion speed and a decreased rate of NO formation.

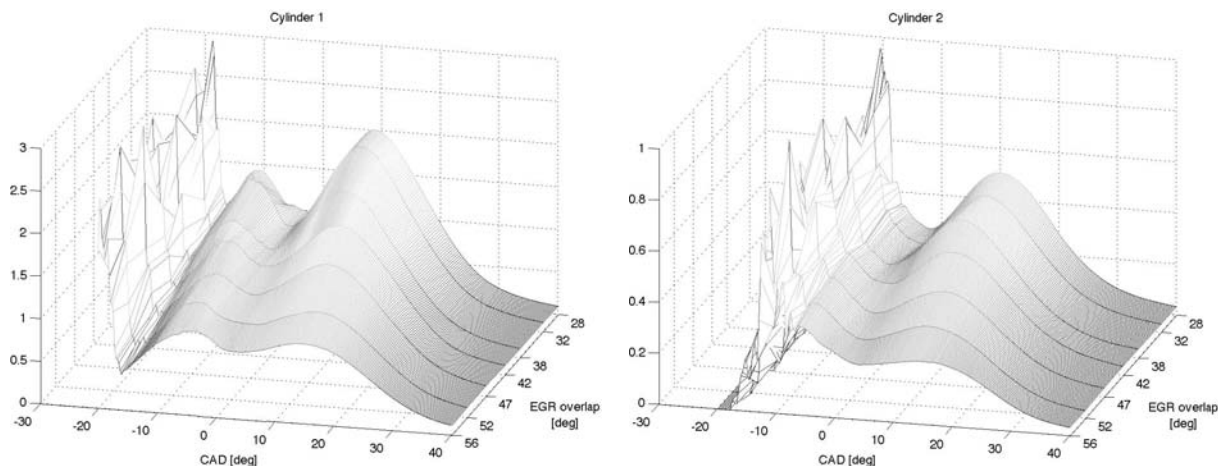


Figure 3.8: 3D plots of the averaged ionization curves measured in cylinder 1 and cylinder 2 for the EGR sweep.

### 3.4.3 Engine load

The throttle angle and the intake manifold pressure  $p_{im}$ , which directly relates to the engine load, control the air supply to the cylinders for SI engines. After the air passes the throttle, it is mixed with fuel in the intake system and then the air-fuel mixture is drawn into the cylinder due to pressure differences induced by the downwards movement of the piston. The most commonly used method today for controlling the mass ratio between the air and fuel in the mixture ( $\lambda$ ) is letting the driver control the air supply with the throttle through the ECU. A step input from the throttle results in an increased flow of air which builds up the intake manifold pressure. The air temperature sensor, the air flow sensor, and the  $\lambda$  sensor are then used by the engine control system to determine the corresponding increase of fuel to retain the mixture at stoichiometric conditions and the result of this is that the output power of the engine increases.

The following sweep of the engine load parameter was performed by changing the intake manifold pressure:

40 50 60 70 80 90 100 110 120 130 140 [kPa]

To be able to study the changes of the averaged ionization current and cylinder pressure only the first part of the sweep 40-80 kPa was plotted in figure 3.9. For higher loads the SA is increased towards TDC by the ECU to avoid knock which would make the figure hard to read. The reason for this is that an increased engine load results in a higher combustion temperature and a faster burn rate which is compensated by the increased SA. This makes the measurements dependant on both the engine load and SA.

The ionization currents for the entire engine load sweep are plotted in figure 3.10. From the figures it can be seen that during the first part of the sweep, the amplitude of the flame front phase increases and the higher combustion temperature leads to an increased rate of NO formation and a greater thermal peak. In the last part of the sweep when the SA is increased by the ECU, the combustion temperature is lowered and the amplitude of the cylinder

pressure and ionization current decreases. If the SA would be kept constant the amplitude of the curves would be increasing for the whole sweep.

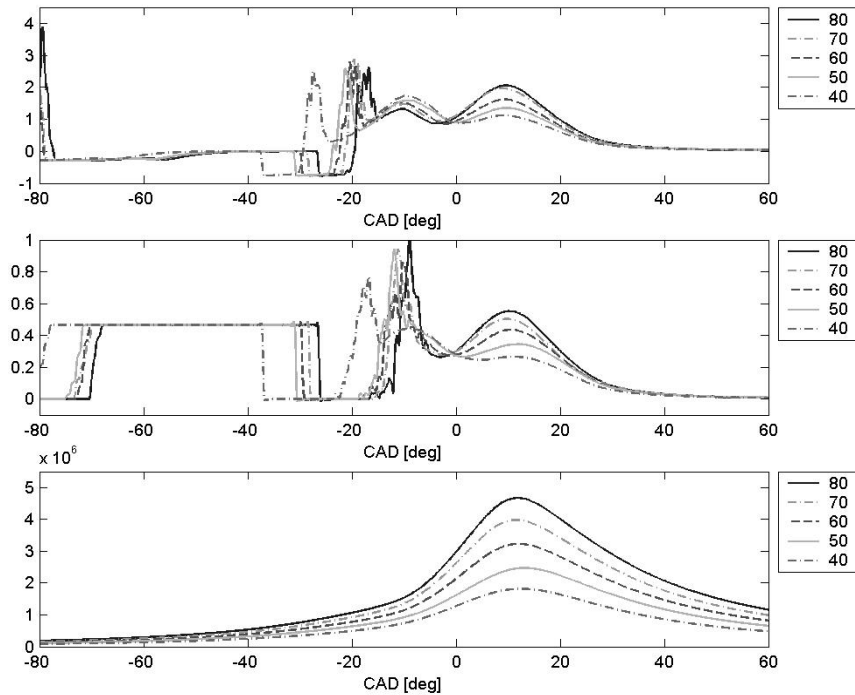


Figure 3.9: An engine load sweep was performed while the engine was operated under the conditions described in table 3.2. Top: The averaged ionization curve measured in cylinder 1. Middle: The averaged ionization curve measured in cylinder 2. Bottom: The averaged cylinder pressure measured in cylinder 2.

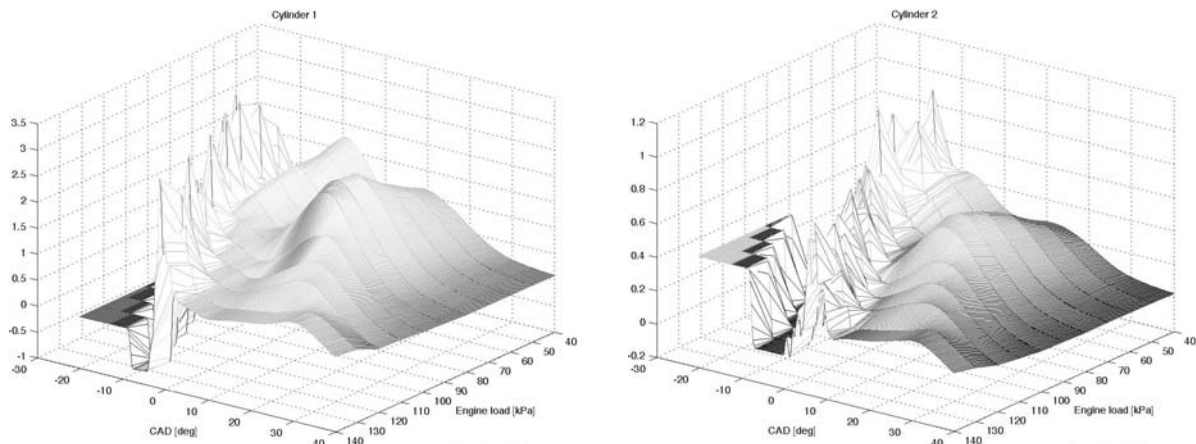


Figure 3.10: 3D plots of the averaged ionization curves measured in cylinder 1 and cylinder 2 for the engine load sweep.

### 3.4.4 Engine speed

Engines produce power by combusting air and fuel. The higher the engine speed, the more power it can produce by combusting more air and fuel. When the speed of an engine increases it becomes less efficient at bringing in air so the output power does not increase linearly with the engine speed. The reasons for this is due to inertia effects in the intake and exhaust systems and flow losses as air velocity increases in the manifolds and ports. In supercharged

engines the output power is increased by increasing the intake air density which results in an increased amount of air into the cylinder. The level of compression and the increase of output power for supercharged engines are primarily limited by engine knock.

The following sweep of the engine speed parameter was performed:  
1200 1500 2000 2500 3000 3500 4000 [rpm]

The averaged ionization current and cylinder pressure from the engine speed sweep can be studied in the figures 3.11 and 3.12. When the engine speed increases so does the amplitude

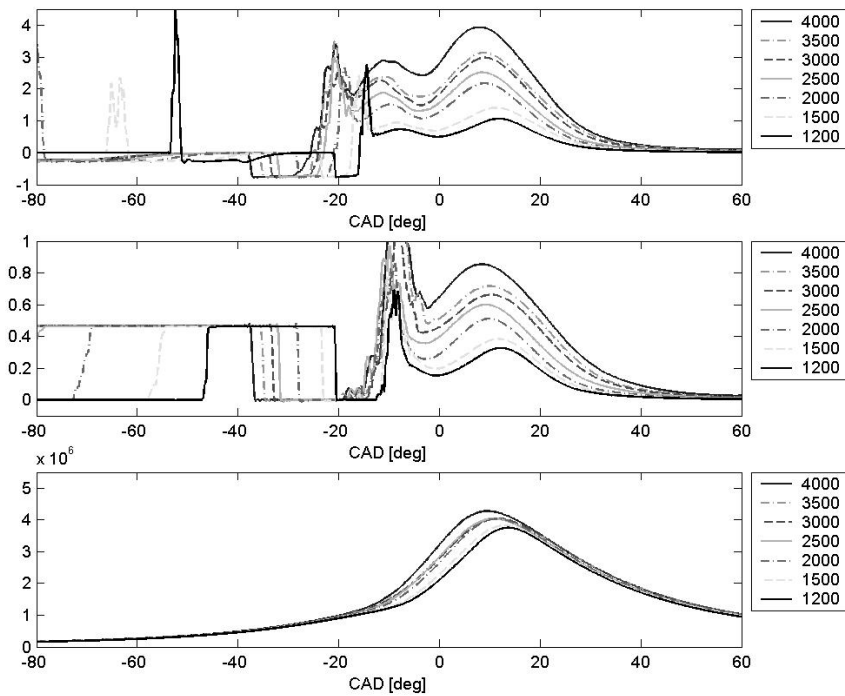


Figure 3.11: An engine speed sweep was performed while the engine was operated under the conditions described in table 3.2. Top: The averaged ionization curve measured in cylinder 1. Middle: The averaged ionization curve measured in cylinder 2. Bottom: The averaged cylinder pressure measured in cylinder 2.

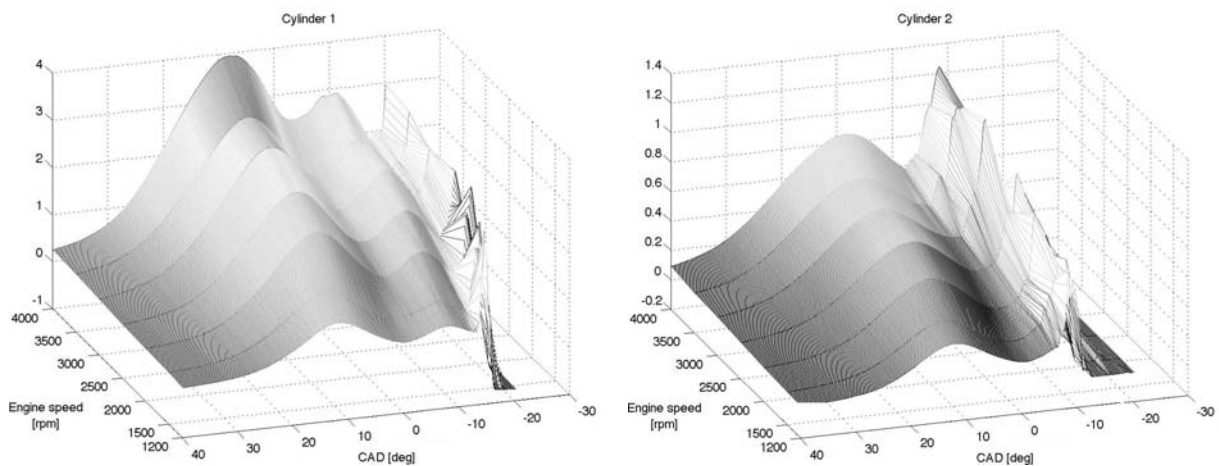


Figure 3.12: 3D plots of the averaged ionization curves measured in cylinder 1 and cylinder 2 for the engine speed sweep.

of the curves. From the averaged ionization curves it can be seen that the ECU advances the SA away from the TDC as the engine speed increases which makes the measurement dependant on both engine speed and SA. The reason for this behaviour is that the time it takes for the air-fuel mixture contained in the cylinder to fully ignite and burn is approximately the same regardless of engine speed. When the engine speed is increased the time available for the combustion to take place decreases. To compensate for this the combustion process must start earlier and the SA is therefore decreased by the ECU.

### 3.4.6 SA

In conventional SI engines the air and fuel are mixed together in the intake system, inducted through the intake valve into the cylinder and then ignited by a spark discharge. The point of ignition is called spark advance (SA) and its timing directly influences several engine outputs such as torque, emission levels, cylinder pressure and ionization current. The aim for the SA is to initiate a stable combustion at a position that maximises the output torque (MBT timing), fulfils emission requirements and prevents the engine from being destroyed by knock.

The following sweep of the SA parameter was performed:  
-45 -40 -35 -30 -25 -20 -15 -10 -5 0 [deg]

The results of the SA sweep can be seen in the figures 3.13 and 3.14. The maximum amplitude of the curves occurs for the highest combustion temperature when the cylinder pressure maximum is positioned nearest the TDC for SA -45 CAD. From the figures it can be seen that when the SA is increased towards TDC, the combustion temperature decreases and the magnitude of the curves declines as a result of this.

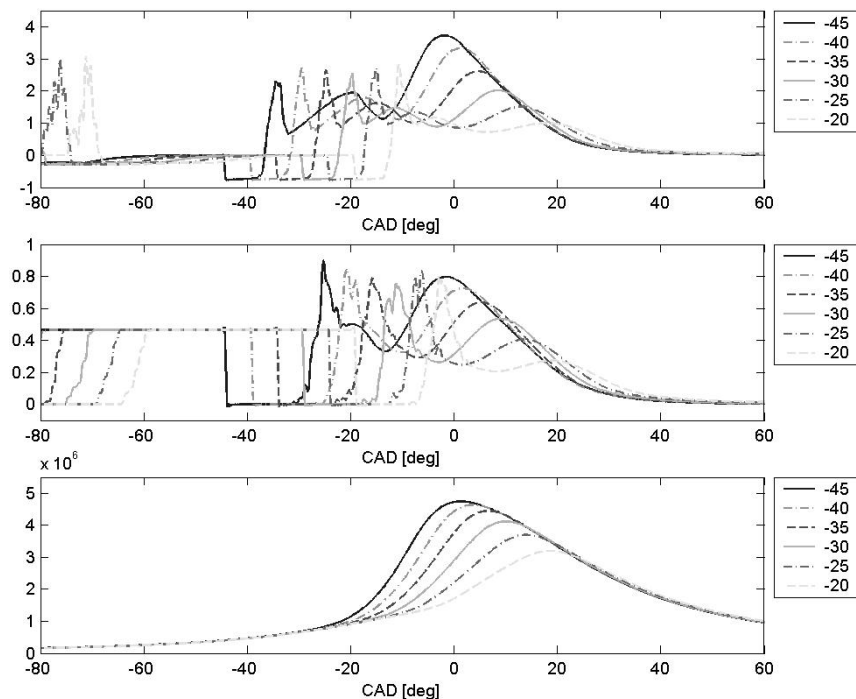


Figure 3.13: A SA sweep was performed while the engine was operated under the conditions described in table 3.2. Top: The averaged ionization curve measured in cylinder 1. Middle: The averaged ionization curve measured in cylinder 2. Bottom: The averaged cylinder pressure measured in cylinder 2.

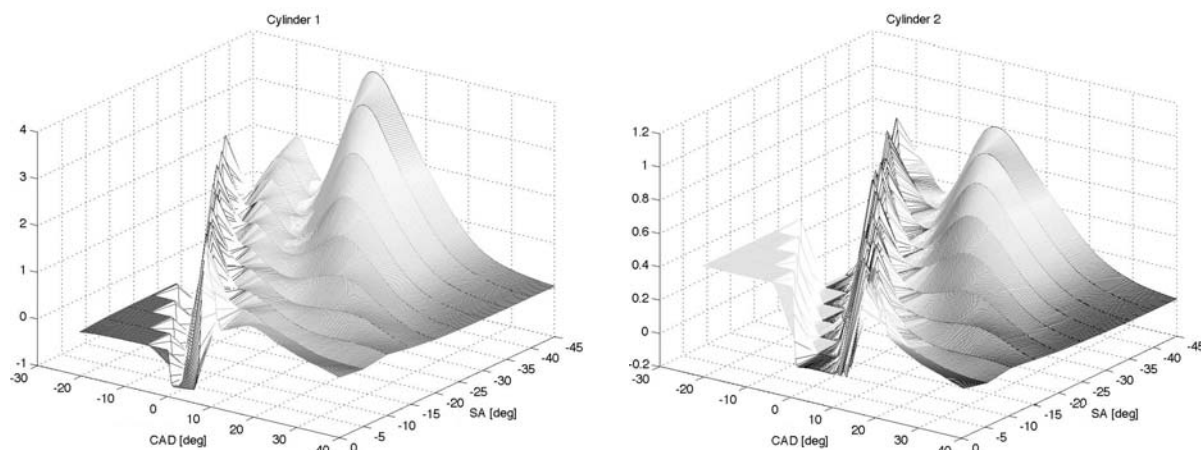


Figure 3.14: 3D plots of the averaged ionization curves measured in cylinder 1 and cylinder 2 for the SA sweep.

### 3.5 Influence of fuel additives

All modern gasoline fuels contain metallic additives which are added to increase the octane number and to lubricate, clear and protect valve and valve seats. The octane number is a practical measurement of a fuel's resistance to knock. A higher octane number means a greater resistance to knock. Increasing the octane number in a fuel is a cheaper way to avoid knock than changing the hydrocarbon composition by refinery processing. The most effective antiknock additive known is lead which was used during a long time until the toxic side effects on the environment was discovered and exhaust gas after-treatment through catalyst became an issue. Since then lead free gasoline have been developed and examples of metallic additives and impurities found in fuel today can be seen in table 3.4. For each additive the ionization energy and the approximate maximum levels in gasoline are given.

Material	Ionization energy (eV)	Max levels in gasoline
K (Potassium)	4,3440	10-15 ppm (valve seat protection)
Na (Sodium)	5,1341	10-15 ppm (valve seat protection)
Pb (Lead)	7,4167	Still used in some markets, up to 300 ppm
Mn (in MMT)	7,4340	approx. 5-15 ppm (octane booster)
Fe (in Plutocen)	7,9024	approx. 5-50 ppm Plutocen (octane booster)
S (Sulfur)	10,3600	0-50 ppm in Europe, 0-150 in US, Rest $\leq$ 3000 ppm
P (Phosphorus)	10,4867	approx 20 ppm (valve seat protection)

Table 3.4: Examples of metallic additives and impurities found in fuel.

In engine oil there are a number of metallic additives that have low ionization energy. If an engine has a high oil consumption those additives might affect the ion current measurements. Examples of metallic additives in engine oil can be seen in table 3.5.

No investigation of how fuel additives affect the ionization current could be made because the design of the fuel supply system in the measurement system made it impossible. Instead the results from [20] and [23] is summarized. The additives Na and K are the easiest additives to ionize thermally due to their low ionization energy. From experiments their effects on the ionization current have been studied. In [20] they increased the absolute signal level of the

ionization current. The typical two peak shape was perturbed to yield a single peak. The phasing of the ionization current appears however to remain intact. In [23] a small amount of Na was added with the result of amplifying the thermal peak four times compared with the case without Na. These results give a hint of what influence fuel additives have on the ionization current. Fuel additives and fuel quality are a concern because they are not under the control of the engine manufacturer. The fuel quality varies from one country to another, gasoline companies may add different additives to their fuel and it is possible to buy additives at the local gas station to mix with the fuel after filling up. To be able to implement a successful closed-loop control of the SA for MBT timing, it is therefore important to make a thorough investigation how the correlation between combustion descriptors estimated from the cylinder pressure and the ionization current change and how robust the algorithms are when different sorts of fuel additives are used.

Material	Ionization energy (eV)	Levels in engine oil
Ca (Calcium)	6,1132	< 4000 ppm
Mo (Molybdenum)	7,0924	< 200 ppm
Mg (Magnesium)	7,6462	< 1200 ppm
B (Boron)	8,2980	< 400 ppm
Zn (Zinc)	9,3942	< 1500 ppm
P (Phosphorus)	10,4867	< 1500 ppm
S (Sulfur)	10,3600	< 5000 ppm

*Table 3.5: Examples of metallic additives in engine oil.*



## Chapter 4

# Implementation, estimation and result

A number of combustion descriptors for closed-loop control of the SA for MBT timing exists. In chapter 2 the combustion descriptors PPP, 50%MFB and MAMFB were presented. Since cylinder pressure sensors are not an option the descriptors have to be estimated from the ionization current. The PPP is estimated from the peak in the post flame phase while the 50%MFB and MAMFB are estimated from the curvature of the peak in the flame front phase. When investigating how the ionization current is affected by changes of the engine operating parameters in section 3.4, it was discovered that the peak in the flame front phase was destroyed by the prolonged coil ringings when the ignition system in cylinder 2 with a long ignition duration was used. No attempt to estimate the combustion descriptors 50%MFB and MAMFB was therefore made. The focus was instead aimed towards implementing and improving the algorithms which estimate the PPP from the ionization current.

### 4.1 PPP estimating algorithms

There exist several different techniques to estimate the PPP from the ionization current; for example fuzzy logic, neural networks, curve modelling and double derivate approximation. The techniques explained in this thesis are ANN, Gaussian fit, SQUAD aka Peakfinder and DD.

#### 4.1.1 ANN

In [23] the PPP is estimated by using an artificial neural network (ANN) of the multilayer perceptron (MLP) form [25]. ANN:s are generic models that often are used when a physical model is unknown, incomplete or difficult to implement. The strength and weakness of ANN:s is their ability to adapt to training data without having any knowledge of a existing relationship between the input and the output data. In this case the input data is a compressed ionization current data vector achieved by using principal component analysis (PCA) and the output data is the PPP. The MLP is shaped after the input data and the desired output data and is thus sensitive to signal levels and the dimension of the input data. A suitable preprocessing of the ionization current is therefore required for the model to perform well. Although being a

complex structure requiring hours of training before usage, the realtime operation of an MLP requires a small amount of computation power and it is therefore very fast. Problems can occur when the input data differs too much from the data that was used when training the ANN. The difficulty to interpret the trained ANN model and predict the output data for those cases requires some sort of model to fall back on. One solution is to combine the ANN model with a static lookup table.

The combination of collecting training data for different operating conditions, fuel additives, engine designs and then choosing the right set of training data and finally evaluating the ANN with the right set of input data is too extensive and time consuming for this thesis.

### **4.1.2 Gaussian fit**

The Gaussian fit algorithm presented in [12] and further evaluated by [23, 24, 26, 27] is based on the assumption that the flame front and post flame phase of the ionization current can be modelled by using a sum of two or three Gaussian curves where the peak of one of the curves coincides with the PPP. The algorithm is nonlinear and the parameters are tuned by iteratively least square fitting the model to the ion current which makes it time consuming. The Gaussian fit algorithm will perform well if the measured ionization current signal resembles a nice superposition of two or three Gaussians. But if the ionization current takes a different shape with more or less peaks which is common due to the always present cycle-to-cycle variations or if the PPP does not coincide with any of the Gaussian peak, then the performance of the algorithm will be poor. The effect of the stochastic cycle-to-cycle variations in the signal can be decreased by averaging the ionization current over several cycles with 10 cycles being an optimum number according to [1].

Averaging the ionization current and iteratively least square fitting the parameters of the model in realtime when driving on the highway is very demanding for the ECU. This is the primary reason why the Gaussian fit algorithm was not further investigated here.

### **4.1.3 SQUAD aka Peakfinder**

In [26] another curve fitting algorithm designed to find the PPP from the peak in the post flame phase is presented. Instead of trying to model the whole ionization current, a backwards sliding window technique is used to successively do local models of the ionization current by using a second order polynomial. The Peakfinder or Sliding Quadratic Fit (SQUAD) algorithm [23] starts at the end of the post flame phase of the ionization current and stops when the flame front phase is considered to be found. Detecting the flame front is necessary to avoid estimating the PPP from the wrong peak. To detect the flame front phase a threshold value on the second derivatives of the local models are used and then the PPP is estimated from the model which has the smallest second derivative.

The performance of the algorithm have been compared against the ANN and Gaussian fit algorithm in [26, 27]. The results from the articles can be summarized as that the best candidate for PPP feedback control is the SQUAD algorithm due to robustness towards operating conditions under low engine loads when the post flame peak is small or even missing and due to the ability to provide unbiased estimates. A drawback with using the second derivative to detect the flame front phase is that the algorithm becomes sensitive to amplitude changes.

The simplicity to implement the algorithm and its reported good performance when comparing it to the previously mentioned PPP estimating algorithms are the reasons why the algorithm is further investigated in this thesis.

#### 4.1.4 DD

The double difference (DD) algorithm presented in [23] is a further development and simplification of the SQUAD algorithm. According to the authors the objective of a PPP estimating algorithm is not to produce reliable estimates every cycle but to give unbiased estimates on average. This is motivated by the fact that the algorithm is going to be used for closed-loop control where only a fraction of the estimate is used every cycle. With this in mind, it makes little sense to use curve fitting techniques to average out single cycle noise. Instead of fitting local models to the ionization current and then use their second derivate to find the post flame phase and the PPP, a double difference is directly estimated from the ionization current thus avoiding the introduction of local models which speeds up the algorithm considerably. An improvement of the flame front phase detection is made for the cases where the SQUAD algorithm performed poorly.

The DD algorithm is less complex, fast and according to [23] it performs better than the ANN and SQUAD algorithm and will therefore also be investigated in this thesis.

## 4.2 Implementation

The SQUAD and DD algorithm both estimates the PPP from the post flame peak but uses different approaches to do so. The SQUAD algorithm uses locally fitted models and their second derivates while the DD approximates the second derivate by using a double difference directly from the ionization current. Both rely on the curvature of the ionization current to be able to detect the flame front phase and to produce valid PPP estimates. Covering all possible curvature variations is impossible since unmeasurable disturbances like fuel additives exist. The proposed solution in this thesis removes this dependency by using an engine operating point dependant part of the ionization current instead of relying on the curvature of the ionization current. This new technique is described in section 4.2.3 together with the simplified SQUAD and DD algorithms.

### 4.2.1 SQUAD

The local model that successively is fitted to the ionization current signal  $i(\theta)$  is a second order polynomial

$$\hat{i}(\theta; p_0, p_1, p_2) = p_0 + p_1\theta + p_2\theta^2 \quad (4.1)$$

where  $\theta$  is the CAD. The algorithm operates on the ionization current in the interval 0-35 CAD ATDC [27] using a local backwards sliding window technique. The model parameters  $p_0$ ,  $p_1$  and  $p_2$  are estimated to locally fit the model to the ionization current for each window. Since there are three unknown parameters it is necessary to have a sliding window of at least 3 CAD. In order to reduce noise effects a window length of 5 CAD is chosen [26]. The least square problem that is solved when estimating the parameters for each window is

$$\min_{p_0, p_1, p_2} \sum_{k=1}^5 \left[ i(\theta_k) - \hat{i}(\theta_k; p_0, p_1, p_2) \right]^2 \quad (4.2)$$

To avoid finding the wrong peak, the fact that the flame front peak typically has a much sharper slope to climb than the post flame peak is used. The second derivate of the local models

$$\frac{\partial^2 \hat{i}(\theta)}{d\theta^2} = 2p_2 \quad (4.3)$$

is therefore used to detect when the flame front phase ends. When the second derivate  $2p_2$  of a local model exceeds an optimised fixed threshold value the flame front phase is considered to be found. The local model with the smallest second derivate is then chosen as the one containing the PPP. For this local model an estimate  $\hat{\theta}_{PPP}$  of the PPP is obtained as the local maximum where the first derivate is zero.

$$\frac{d\hat{i}(\theta)}{d\theta} = 0 \Rightarrow \hat{\theta}_{PPP} = -\frac{p_1}{2p_2} \quad (4.4)$$

A final check is then made to constrain the estimated PPP value within the validity range of the locally estimated model

$$\hat{\theta}_{PPP} = \min\left[\max\left[\theta_1, \hat{\theta}_{PPP}\right], \theta_5\right] \quad (4.5)$$

where  $\theta_1$  is the start CAD of the window and  $\theta_5$  the end CAD of the window belonging to the local model with the smallest second derivate.

The SQUAD algorithm is summarised as:

1. Use the ionization current in the interval 0-35 CAD ATDC.
2. Implement a backwards sliding window technique with a window length of 5 CAD. The first window is between  $\theta_1 = 31$  and  $\theta_2 = 35$  CAD. For each window:
  - a. Estimate a local model of the ionization current (4.1) using (4.2).
  - b. Stop when the second derivate  $2p_2$  of the estimated local model exceeds an optimised fixed threshold or the beginning of the ionization current is found at 0 CAD.
3. Find the local model with the smallest second derivate  $2p_2$ . For that model:
  - a. Find the PPP estimate  $\hat{\theta}_{PPP}$  with (4.4).
  - b. Check that  $\hat{\theta}_{PPP}$  is within the validity range of the local model (4.5).
4. Return  $\hat{\theta}_{PPP}$ .

#### 4.2.2 DD

Calculate the approximation of the first and second derivate of the ionization current for the interval 1-30 CAD ATDC [23] by using a forward difference approximation

$$d(\theta) = i(\theta + 1) - i(\theta), \theta = 1, 2, \dots, 29 \quad (4.6)$$

$$dd(\theta) = d(\theta) - d(\theta - 1), \theta = 2, 3, \dots, 29 \quad (4.7)$$

where  $\theta$  is the CAD. The algorithm is very fast since only  $29 + 28 = 57$  subtractions are needed to calculate the second derivate of a given ionization current. The DD algorithm is an improvement and simplification of the earlier mentioned SQUAD algorithm which according to the authors performs poorly for the cases when the amplitude of the ionization current is too large, for example at high engine loads or when fuel additives are present. To improve the performance during these operating conditions, a test to detect if the amplitude of the ionization current is over or under a optimised threshold  $i_0$  at a chosen CAD point  $\theta_0$  is introduced.

For ionization currents with small amplitudes  $i(\theta_0) \leq i_0$ , the end of the flame front phase  $\theta_f$  is first detected by sorting out all of the second derivatives that exceeds an optimised threshold  $dd_0$ . Then the second derivative which occurs last during the combustion process is considered to be the end of the flame front phase.

$$\theta_f = \max \arg[dd(\theta) > dd_o] \quad (4.8)$$

The PPP estimate  $\hat{\theta}_{PPP}$  is then obtained by finding the CAD for the smallest second derivative of the ionization current during the post flame phase.

$$\hat{\theta}_{PPP} = \arg \min_{\theta > \theta_f} dd(\theta) \quad (4.9)$$

For ionization currents with large amplitudes  $i(\theta_0) > i_0$ , the  $\hat{\theta}_{PPP}$  is estimated as the CAD where the ionization current has its maximum value.

$$\hat{\theta}_{PPP} = \arg \max i(\theta) \quad (4.10)$$

The DD algorithm is summarised as:

1. Use the ionization current in the interval 0-30 CAD ATDC.
2. Calculate the approximate second derivative  $dd(\theta)$  with (4.6) and (4.7).
3. At a chosen CAD point  $\theta_0$ . Test if the amplitude of the ionization current  $i(\theta_0)$  is over or under an optimised threshold  $i_0$ .
  - a. If  $i(\theta_0) \leq i_0$ , the end of the flame front phase  $\theta_f$  is detected with (4.8). Then  $\theta_f$  is used with (4.9) to obtain the PPP estimate  $\hat{\theta}_{PPP}$ .
  - b. If  $i(\theta_0) > i_0$ , the  $\hat{\theta}_{PPP}$  is estimated as the CAD where the ionization current has its maximum value (4.10).
4. Return  $\hat{\theta}_{PPP}$ .

### 4.2.3 Improvement

The Achilles heel of both the SQUAD and DD algorithm is the dependency of the curvature of the ionization current to detect the flame front phase. A fixed threshold value is used for all operating points and this makes the algorithms sensitive to amplitude changes. Covering all possible amplitude variations is impossible with a fixed threshold. According to the authors the algorithms perform poorly for high engine load, high EGR rate and when fuel additives are present. The engine load can be measured and accounted for, but EGR and fuel additives are a concern since they are hard to measure. As mentioned earlier in section 3.5 fuel additives can change the magnitude of the ionization current and perturb the typical two peak shape to yield a single peak which would deteriorate the performance of the algorithms. It is also mentioned that the fuel additives do not affect the phasing of the ionization current [20].

The proposed solution in this thesis is to use an engine operating dependant part of the ionization current instead of relying on the curvature of the ionization current. The idea is based on using a fixed end position and an engine operating point dependent start position which depends on the parameters engine load, engine speed and SA as illustrated in figure 4.1. The motivation for this is when the results of the different engine parameter sweeps from table 3.3 in section 3.4 are studied, the three engine operating parameters which affect the phasing of the ionization current are the engine load, engine speed and SA. Since they offset the ionization current, the engine operating point dependant start position must be able to

adapt to these operating parameters and is therefore made dependant of them.

$$start(N, p_{im}, SA) \quad (4.11)$$

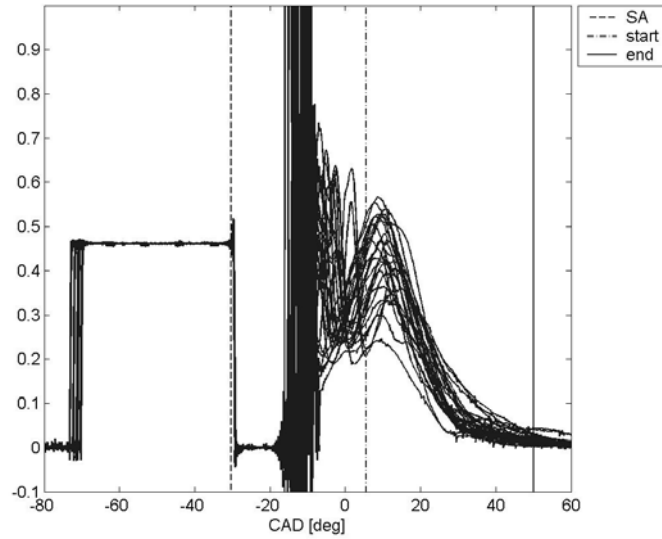


Figure 4.1: The engine operating point dependant start position at 5 CAD and the fixed end position at 50 CAD for 25 measured cycles of the ionization current when the engine was operated at  $N = 2000\text{rpm}$ ,  $p_{im} = 60\text{kPa}$  and  $SA = -30.4\text{ CAD}$ .

When a fixed part of the ionization current is used for a given engine operating point, the SQUAD and DD algorithm can be simplified. The step 2b to avoid estimating the PPP from the wrong peak by detecting the flame front phase is removed for the SQUAD algorithm. Since the curvature of the ionization current no longer is used, there is no need to detect if the amplitude is too large. The test in step 3 is therefore removed for the DD algorithm. The simplified SQUAD and DD algorithm can be summarised as:

Simplified SQUAD algorithm:

1. Use the ionization current in the interval  $[start(N, p_{im}, SA) \text{ end}]$ , where  $\text{end} = 50\text{ CAD}$ .
2. Implement a backwards sliding window technique with a window length of 5 CAD. The first window is between  $\theta_1 = 46$  and  $\theta_2 = 50\text{ CAD}$ . For each window:
  - a. Estimate a local model of the ionization current (4.1) using (4.2).
3. Find the local model with the smallest second derivate  $2p_2$ . For that model:
  - a. Find the PPP estimate  $\hat{\theta}_{PPP}$  with (4.4).
  - b. Check that  $\hat{\theta}_{PPP}$  is within the validity range of the local model (4.5).
4. Return  $\hat{\theta}_{PPP}$ .

Simplified DD algorithm:

1. Use the ionization current in the interval  $[start(N, p_{im}, SA) \text{ end}]$ , where  $\text{end} = 50\text{ CAD}$ .
2. Calculate the approximate second derivate  $dd(\theta)$  with (4.6) and (4.7).
3. The PPP estimate  $\hat{\theta}_{PPP}$  is then obtained by finding the CAD for the smallest second derivate of the ionization current.
$$\hat{\theta}_{PPP} = \arg \min dd(\theta)$$
4. Return  $\hat{\theta}_{PPP}$ .

### 4.3 Parameter estimation

The estimation of the engine operating point dependant start parameter (4.11) is performed on a data set which was measured in cylinder 1 for the operating conditions presented in figure 4.2. The data set consists of 23 different operating points with 100 measured cycles each where the load and speed of the engine were changed. By using the default EGR setting  $28^\circ$  and letting the ECU determine the  $\lambda$  and SA, normal driving conditions was tried to be imitated. The corresponding SA values determined by the ECU can be seen in table 4.1.

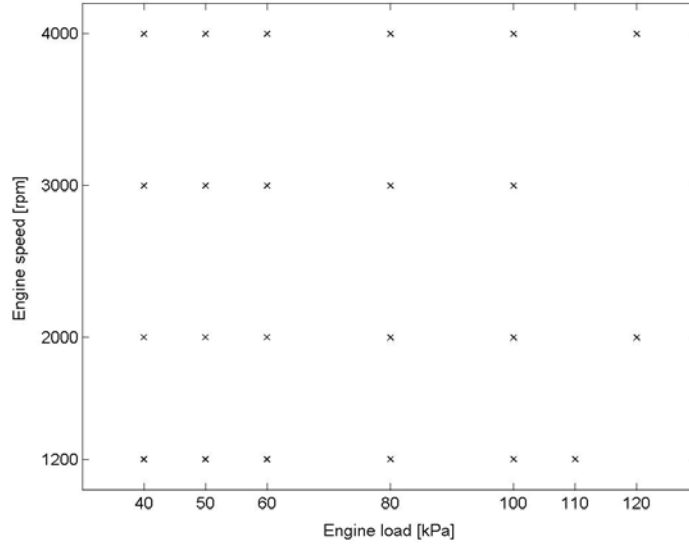


Figure 4.2: Data set of 23 measurements where the load and speed of the engine were changed. The corresponding SA values determined by the ECU can be seen in table 4.2.

For a given engine operating point, the start parameter which results in the combination of smallest root mean square (RMS) and bias error when estimating the PPP is saved. The RMS and bias error were calculated with

$$RMS = \sqrt{\frac{1}{N} \sum_{k=1}^N [\theta_{PPP}(k) - \hat{\theta}_{PPP}(k)]^2} \quad (4.12)$$

$$Bias = \frac{1}{N} \sum_{k=1}^N \theta_{PPP}(k) - \hat{\theta}_{PPP}(k) \quad (4.13)$$

where the  $\theta_{PPP}$  is estimated with (2.2) and the  $\hat{\theta}_{PPP}$  is estimated using the simplified SQUAD and DD algorithms described in section 4.2.3. The algorithms operated on single cycles of the ionization current which were sampled with a resolution of 1 CAD and a 4<sup>th</sup> order lowpass butterworth filter with the optimised cutoff frequency 2893Hz was used to zero phase filter the engine operating point dependant part of the ionization current. No measured cycles were removed. The start parameter was estimated from the CAD interval [-5:1:20] for both of the algorithms. The result of the start parameter estimation and the estimation accuracy of the algorithms on the data set are presented in table 4.1 and 4.2. The conditions just described are also later used together with the estimated start parameter in section 4.4 and 4.5, where the estimation accuracy and robustness of the algorithms are evaluated on a data set which was measured at the same time in cylinder 2.

It can be seen in table 4.1 that for high engine loads the SA is increased towards TDC by the ECU to avoid knock. The reason for this is that an increased engine load results in a higher combustion temperature and a faster burn rate which is compensated by the increased SA. When comparing the start parameter estimated by the SQUAD and DD algorithm, minor differences can be seen. The parameter estimation differs in 6 operating points of 23 by 1-2 CAD. The explanation for this lies in the different techniques used by the algorithms and the number of measured cycles in the used operating points. If more cycles were measured for each operating point the estimation differences would decrease.

N [rpm]	$p_{im}$ [kPa]	SA [deg]	SQUAD	DD
			Start [deg]	Start [deg]
1200	40	-32.3	6	6
1200	50	-25.0	8	9
1200	60	-22.8	8	8
1200	80	-18.3	11	11
1200	100	-12.4	16	16
1200	110	-8.9	18	18
2000	40	-37.4	5	5
2000	50	-31.7	5	5
2000	60	-30.4	5	5
2000	80	-27.4	6	6
2000	100	-20.6	12	13
2000	120	-13.4	14	15
3000	40	-40.0	1	3
3000	50	-40.0	5	5
3000	60	-36.6	5	5
3000	80	-33.3	5	5
3000	100	-29.7	7	7
4000	40	-40.0	2	2
4000	50	-40.0	2	2
4000	60	-40.0	3	3
4000	80	-37.6	3	2
4000	100	-33.0	4	4
4000	120	-25.9	7	7

Table 4.1: The estimated start( $N$ ,  $p_{im}$ , SA) parameter from equation (4.11) on the data set measured in cylinder 1 for the SQUAD and DD algorithm.

The estimation accuracy of the algorithms on the data set in table 4.2 reveals a promising result. The overall estimation accuracy of the algorithms is good except in 3 operating points; 3000rpm 40kPa, 4000rpm 40kPa and 4000rpm 50kPa. When comparing the estimation accuracy of the two algorithms, the slower and more complex SQUAD algorithm is found to perform slightly better than the DD algorithm. The mean(abs(RMS)) error for the whole data set is 1.74 CAD for the SQUAD algorithm and 2.0 CAD for the DD while the mean(abs(bias)) is 0.32 CAD for both of the algorithms.

To illustrate the effect of the RMS and bias error on the performance of the algorithms, the best and worst operating points in terms of estimation accuracy for the SQUAD algorithm is plotted in figure 4.3. In the figure the earlier mentioned cycle-to-cycle variations of the combustion process can clearly be seen in the PPP. The operating point where the estimation



accuracy of the SQUAD algorithm is best is at 2000rpm and 100kPa where the RMS error is 0.92 CAD and the bias error is -0.06 CAD. From the top figure 4.3 it can be seen that during this operating point the PPP estimate from the SQUAD algorithm shows a close correspondence to the PPP. In the bottom figure 4.3 the worst operating point for the algorithm can be seen. The performance is severely reduced since the algorithm is continuously over- and underestimating the PPP which leads to a high RMS error.

N [rpm]	P <sub>im</sub> [kPa]	SA [deg]	SQUAD		DD	
			RMS [deg]	bias [deg]	RMS [deg]	bias [deg]
1200	40	-32.3	1.73	-0.09	1.90	-0.35
1200	50	-25.0	1.09	-0.08	1.27	0.02
1200	60	-22.8	1.14	0.45	1.18	0.05
1200	80	-18.3	1.00	0.59	0.87	0.26
1200	100	-12.4	0.93	0.33	1.00	0.22
1200	110	-8.9	1.06	0.58	1.28	0.92
2000	40	-37.4	2.20	-0.13	2.53	-0.33
2000	50	-31.7	1.51	0.44	1.78	0.42
2000	60	-30.4	1.45	0.50	1.53	0.50
2000	80	-27.4	1.17	0.69	1.12	0.42
2000	100	-20.6	0.92	-0.06	0.89	-0.20
2000	120	-13.4	1.31	-0.19	1.90	-0.08
3000	40	-40.0	3.05	-0.30	4.08	0.13
3000	50	-40.0	2.09	0.09	2.40	-0.06
3000	60	-36.6	1.71	-0.06	1.98	-0.20
3000	80	-33.3	1.50	0.43	1.59	0.27
3000	100	-29.7	1.41	0.25	1.36	-0.17
4000	40	-40.0	4.92	-1.16	5.27	-1.07
4000	50	-40.0	2.58	0.16	3.25	0.42
4000	60	-40.0	1.78	-0.16	2.11	0.15
4000	80	-37.6	1.64	-0.03	2.00	-0.06
4000	100	-33.0	1.83	0.31	2.13	0.84
4000	120	-25.9	2.05	-0.16	2.55	0.27
mean(abs)			1.74	0.32	2.00	0.32

Table 4.2: The estimation accuracy of the SQUAD and DD algorithm on the data set measured in cylinder 1 when the estimated start parameter from table 4.1 was used.

The engine operating points where the estimation accuracy of the algorithms is worst are 3000rpm 40kPa, 4000rpm 40kPa and 4000rpm 50kPa. The explanation for this is that the thermal peak is harder to detect for low loads with a slow rate of NO formation due to low combustion temperature in combination with high engine speeds where the different phases of the ionization current merges and becomes harder to distinguish. The mentioned operating points are the worst possible for PPP estimating algorithms. Four examples where the PPP estimation fails are illustrated in figure 4.4. The SQUAD and DD algorithm fails during these operating conditions since the PPP position is not at a peak and therefore can not be detected by the algorithms. The ionization current forms where the performance of the algorithms deteriorates seem to occur more frequently during these engine operation conditions. One solution for improving the performance during these conditions is to use statistical methods [28]. Another possible solution would be to investigate algorithms for estimating the

combustion descriptors 50%MFB and MAMFB. Their estimation accuracy might be better during these operating conditions.

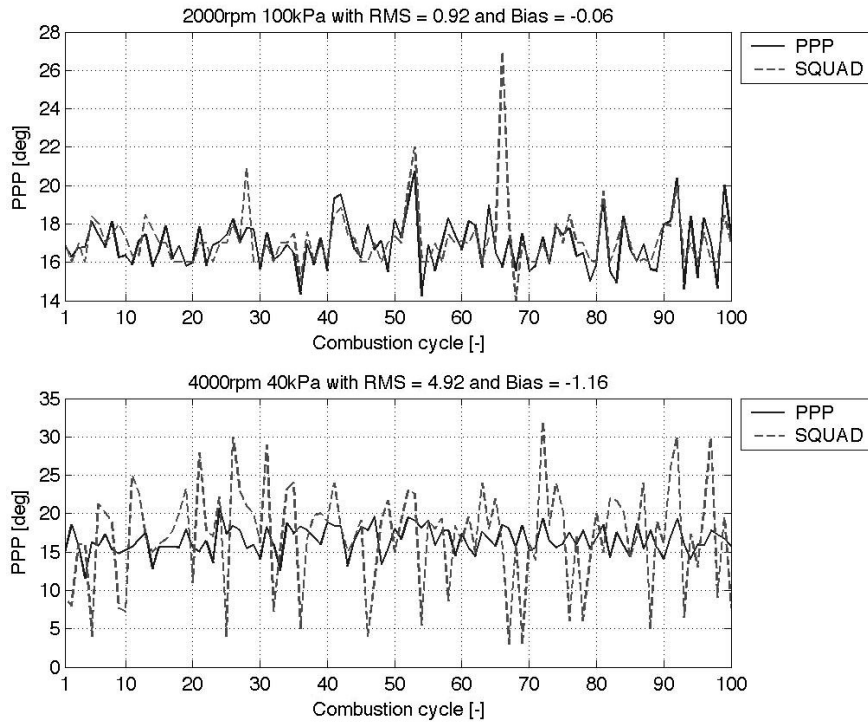


Figure 4.3: The best and worst operating points in terms of estimation accuracy on the data set measured in cylinder 1 for the SQUAD algorithm where PPP is the  $\theta_{PPP}$  and SQUAD is the  $\hat{\theta}_{PPP}$ .

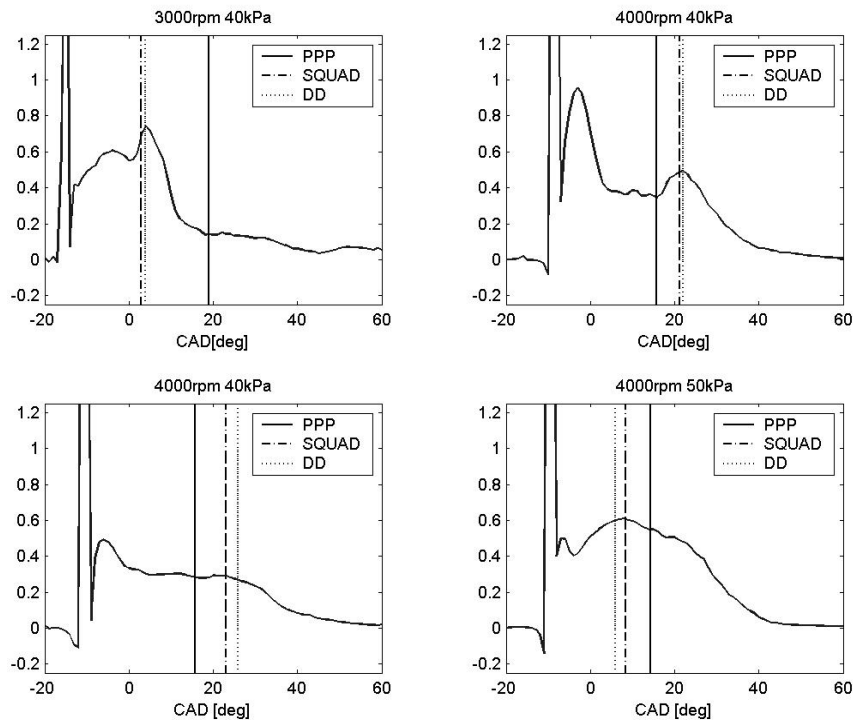


Figure 4.4: Examples of ionization currents where the PPP estimating algorithms are having problems estimating the PPP where PPP is the  $\theta_{PPP}$  and SQUAD and DD is the  $\hat{\theta}_{PPP}$ .

## 4.4 Result

The estimation accuracy of the algorithms presented in table 4.2 on the data set measured in cylinder 1 could be misleading since the used start parameter from equation (4.11) was estimated on the same data set. The performance of the algorithms is therefore also investigated on a data set which was simultaneous measured in cylinder 2. The investigation was performed under the same conditions as described in section 4.3 using the estimated start parameter from table 4.1. The result can be studied in table 4.3 and figure 4.5.

N [rpm]	$p_{im}$ [kPa]	SA [deg]	SQUAD		DD	
			RMS [deg]	bias [deg]	RMS [deg]	bias [deg]
1200	40	-32.3	1.49	0.23	1.70	0.26
1200	50	-25.0	1.09	0.42	1.25	0.59
1200	60	-22.8	1.09	0.64	1.20	0.67
1200	80	-18.3	1.10	0.77	0.92	0.36
1200	100	-12.4	0.93	0.42	1.02	0.25
1200	110	-8.9	1.03	-0.06	0.94	0.42
2000	40	-37.4	2.20	-0.50	2.50	-0.70
2000	50	-31.7	1.99	0.55	2.30	0.53
2000	60	-30.4	1.55	0.87	1.57	0.92
2000	80	-27.4	1.36	0.91	1.33	0.71
2000	100	-20.6	1.44	-0.17	1.66	-0.26
2000	120	-13.4	1.66	0.12	2.21	0.07
3000	40	-40.0	4.86	-1.40	5.31	-1.30
3000	50	-40.0	2.31	-0.10	2.49	-0.44
3000	60	-36.6	1.44	0.22	1.69	0.14
3000	80	-33.3	1.27	0.29	1.40	-0.11
3000	100	-29.7	1.33	0.12	1.50	-0.68
4000	40	-40.0	6.67	-0.48	6.91	-0.81
4000	50	-40.0	3.82	-0.37	4.37	-0.55
4000	60	-40.0	1.65	0.22	2.17	0.32
4000	80	-37.6	1.46	0.10	1.84	0.14
4000	100	-33.0	2.93	-0.38	3.42	-0.52
4000	120	-25.9	2.38	0.10	2.98	0.01
mean(abs)			2.05	0.41	2.29	0.47

Table 4.3: The estimation accuracy of the SQUAD and DD algorithm on the data set measured in cylinder 2 when the start parameter estimated on the data set measured in cylinder 1 from table 4.1 was used.

When comparing the mean absolute error mean(abs) from table 4.2 and table 4.3 it can be noticed that the estimation accuracy of the algorithms are worse for the data set measured in cylinder 2 compared with the data set measured in cylinder 1. The differences in the estimation accuracy of the algorithms could be explained by differences in the ignition systems and more important that the start parameter was estimated and adapted to the data set measured in cylinder 1. If more cycles had been measured in each operating point, the start parameter could be estimated and evaluated on the same system. But 50 combustion cycles to perform the start parameter estimation on and 50 cycles to evaluate the estimation accuracy of

the algorithms are too few. A better performance by the algorithms on the data set measured in cylinder 2 would be attained if more cycles were measured for each operating point.

From figure 4.5 it can be confirmed that the worst operating conditions for PPP estimating algorithms are for high engine speeds in combination with low engine loads. As said in the previous section, the estimation accuracy of the algorithms for the worst operating points could be improved by using statistical methods [28] and by performing an investigation if the combustion descriptors 50%MFB and MAMFB could complement the PPP for these operating conditions.

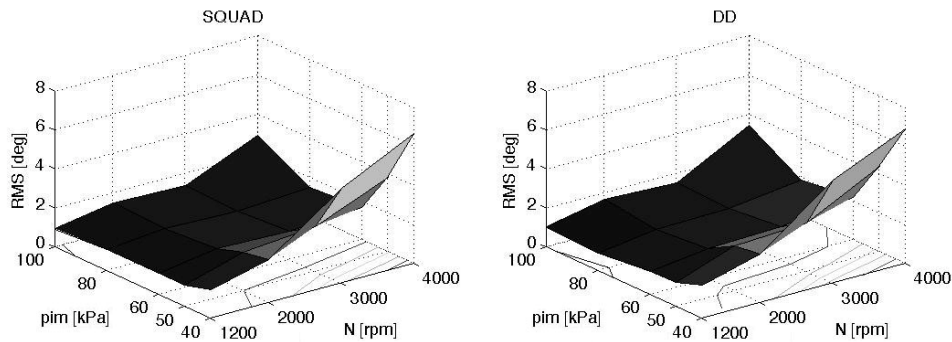


Figure 4.5: 3D plots of the estimation accuracy of the SQUAD and DD algorithm on the result from table 4.3.

## 4.5 Robustness

The goal of this thesis is to investigate if it is possible to estimate the MBT timing from the ionization current for every operating condition of a SI engine where the operating conditions are defined by the engine operating parameters  $\lambda$ , internal EGR, engine load, engine speed and SA. Since the start parameter was made dependable of the engine load, engine speed and SA the robustness of the simplified SQUAD and DD algorithm against  $\lambda$  and EGR needs to be investigated. A robustness test is therefore made on the  $\lambda$  and EGR sweep measured in cylinder 2 from section 3.4 under the same conditions as described in section 4.3. Since the sweeps were performed at the operating point 2000rpm, 70kPa and -29.2CAD where no start parameter has been estimated, the start parameter 5 CAD ATDC from the nearest operating point 2000rpm, 60kPa and -30.4CAD was chosen from table 4.1.

### 4.5.1 $\lambda$ sweep

A  $\lambda$  sweep was performed to test the robustness of the SQUAD and DD algorithm. The same  $\lambda$  data set was used as in section 3.4.1. The results of the  $\lambda$  robustness test can be studied in figure 4.6. The SQUAD algorithm performs slightly better than the DD algorithm in terms of RMS error. The smallest RMS error for both of the algorithms occurs when the ionization current has its amplitude maximum at  $\lambda = 0.88$ . When  $\lambda$  is increased or decreased from this position the RMS error increases as the amplitude of the thermal peak declines and become less distinct which makes it harder for the algorithms to estimate the PPP. Since  $\lambda$  normally is controlled to a narrow band around stoichiometric conditions  $\lambda = 1$  almost no loss of performance will be experienced for this operating point.

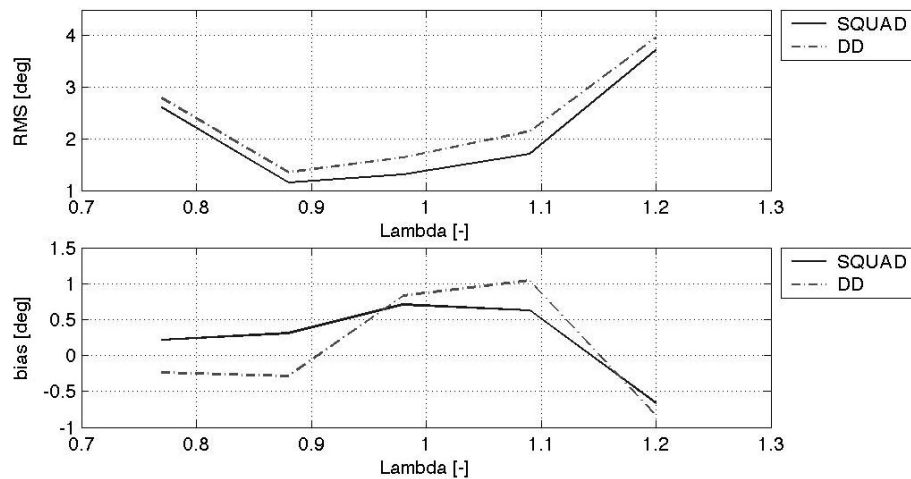


Figure 4.6: The robustness of the SQUAD and DD algorithms for the  $\lambda$  sweep measured in cylinder 2 from section 3.4.1.

#### 4.5.2 EGR sweep

The robustness of the algorithms towards EGR was investigated on the same data set as in section 3.4.2. The amount of recycled gases present in the cylinder is determined by the overlap of the cylinder valves. A greater overlap results in more recycled gases. The performance of the algorithms during the EGR sweep is plotted in figure 4.9. The increasing RMS error seen in top figure 4.7 is most likely due to a lower combustion temperature and rougher engine operation by increased cycle-to-cycle variations when the amount of recycled gases in the combustion chamber increases. This makes it harder to distinguish the thermal peak and the estimation accuracy of the algorithms deteriorates. It can be noticed that the SQUAD algorithm is slightly more robust than the DD algorithm against EGR. When the EGR overlap is increased from the default setting  $28^\circ$  to  $56^\circ$  the RMS error is increased 1.4-1.75 CAD. Under normal operating conditions the EGR setting of the L850 engine is locked to  $28^\circ$  where the estimation accuracy of the algorithms are best, so no loss of performance will be experienced for this operating point.

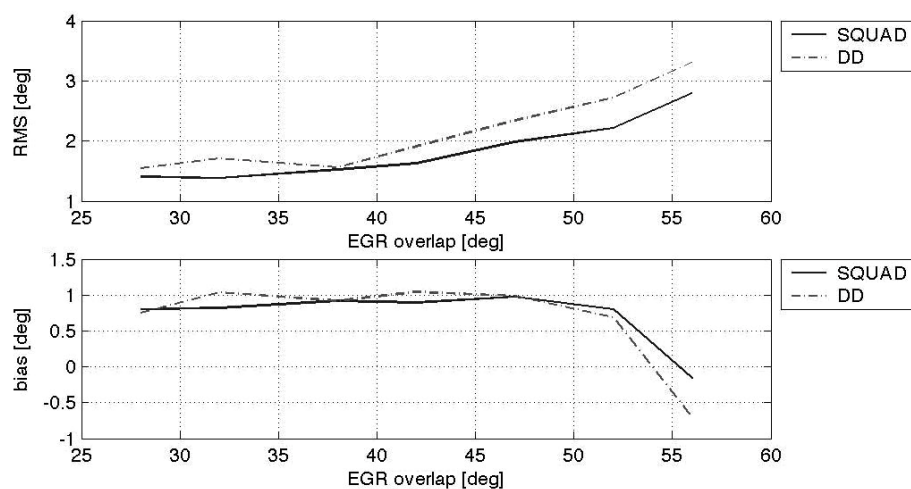


Figure 4.7: The robustness of the SQUAD and DD algorithms for the EGR sweep measured in cylinder 2 from section 3.4.1.



## Chapter 5

### Summary and conclusions

This thesis investigated if it was possible to estimate the MBT timing from the ionization current for every operating condition of a SI engine where the operating conditions are defined by the engine operating parameters  $\lambda$ , internal EGR, engine load, engine speed and SA.

In chapter 2 the four stroke SI engine and the importance of MBT timing are explained. The combustion descriptors PPP, 50%MFB and MAMFB are introduced and an investigation of how much loss of torque a SA and PPP error in CAD from the MBT position corresponds to was made. The combustion descriptors are estimated from the cylinder pressure and can be used for closed-loop control of the SA for MBT timing. Since cylinder pressure sensors are too expensive, the alternative is to estimate the combustion descriptors from the ionization current measured by the already existing spark plug. The ionization current contains information about the cylinder pressure and several publications have shown a high correlation between the combustion descriptors estimated from the cylinder pressure and the ionization current.

In chapter 3 the ionization current was first described and then the influence of fuel additives and the above mentioned engine operating parameters on the amplitude and phasing of the ionization current were investigated for two inductive ignition systems with different ignition durations. During the investigation it was discovered that the peak in the flame front phase was destroyed by the prolonged ringing phenomenon when the ignition system in cylinder 2 with a long ignition duration was used. No attempt to estimate the combustion descriptors 50%MFB and MAMFB from the curvature around of flame front peak was therefore made. The focus was aimed towards implementing and improving the algorithms which estimates the PPP.

In chapter 4 the PPP estimating algorithms ANN, Gaussian fit, SQUAD and DD and their different approaches to estimate the PPP from the post flame peak of the ionization current are presented. A new technique based on the results from section 3.4 is then developed where an engine operating point dependant part of the ionization current is used when estimating the PPP. The technique is based on the fact that only the engine load, engine speed and SA of the above mentioned engine operating parameters affect the phasing of the ionization current. These three parameters are then used to determine an engine operating point dependant start

position of the ionization current used for PPP estimations. The SQUAD and DD algorithms were then complemented with this technique and evaluated. The SQUAD algorithm uses locally fitted models and their second derivate to estimate the PPP while the DD algorithm approximates the second derivate by using a double difference directly from the ionization current. When comparing the estimation accuracy of the two algorithms, the slower and more complex SQUAD algorithm was found to perform slightly better than the DD algorithm. The start parameter was estimated on the data set measured in cylinder 1 and was evaluated on a data set which was measured at the same time in cylinder 2. The mean estimation accuracy of the algorithms on the data set measured in cylinder 2 which consists of 23 different operating points where the engine load, engine speed and SA were changed can be studied in table 4.4. The algorithms operated on single cycles of the ionization current which were sampled with a resolution of 1 CAD. No measured cycles were removed.

	mean(RMS) [deg]	mean( bias ) [deg]
SQUAD	2.05	0.41
DD	2.29	0.47

*Table 4.4: The mean estimation accuracy of the SQUAD and DD algorithms on the data set measured in cylinder 2.*

The overall estimation accuracy of the SQUAD and DD algorithms is promising. The engine operating points where the performance is worst are 3000rpm 40kPa, 4000rpm 40kPa and 4000rpm 50kPa. The explanation for this is that the thermal peak is harder to detect for low loads with a slow rate of NO formation due to low combustion temperature in combination with high engine speeds where the different phases of the ionization current merges and becomes harder to distinguish. The mentioned operating points are the worst possible for PPP estimating algorithms. The estimation accuracy of the algorithms for these conditions could be improved by using statistical methods [28] and by performing an investigation if the combustion descriptors 50%MFB and MAMFB could complement the PPP.

Last the robustness of the simplified SQUAD and DD algorithm against  $\lambda$  and EGR was investigated on the sweeps from section 3.4. The conclusions are that almost no loss of performance will be experienced during normal operating conditions when  $\lambda$  is controlled around stoichiometric conditions  $\lambda = 1$  and the EGR setting of the L850 engine is locked to 28°. This is a promising result which needs to be investigated for more operating points before any general conclusions can be drawn.

## 5.1 Future work

The suggested areas for future work are:

- When investigating how the ionization current is affected by changes of the engine operating parameters in section 3.4, it was discovered that the peak in the flame front phase was destroyed by the prolonged coil ringings when the ignition system in cylinder 2 with a long ignition duration was used. No attempt to estimate the combustion descriptors 50%MFB and MAMFB from the curvature of flame front peak was therefore made. An investigation could however be made by using the data set measured in cylinder 1 where an ignition system with a short ignition duration was used.



- To be able to implement a closed-loop control of the SA for MBT system, it is important to make an investigation of how the correlation between combustion descriptors estimated from the cylinder pressure and the ionization current change and how robust the algorithms are when different sorts of fuel additives are used.
- It was shown in figure 4.6 that for the operating conditions where the performance of the PPP estimating algorithms was worst, the shape of the ionization current made it hard to estimate the correct information. To improve the performance of the algorithms during these operating conditions statistical methods can be used [28]. Another possible solution would be to investigate algorithms for estimating the combustion descriptors 50%MFB and MAMFB. Their estimation accuracy might be better during these operating conditions.



## References

- [1] Lars Nielsen and Lars Eriksson.  
Course material Vehicular Systems  
Vehicular Systems, ISY, Linköping Institute of Technology 2005.
- [2] Lars Eriksson.  
Spark Advance for Optimal Efficiency  
Technical paper 1999-01-0548, Society of Automotive Engineers (SAE), 1999.
- [3] John B. Heywood.  
Internal Combustion Engine Fundamentals  
McGraw-Hill series in mechanical engineering. McGraw-Hill. ISBN 0-07-100499-8,  
1988.
- [4] M. Hubbard, P.D. Dobson and J.D. Powell.  
Closed loop control of spark advance using a cylinder pressure sensor.  
Journal of Dynamic Systems Measurement and Control, Pages 414-420, December  
1976
- [5] Guoming G. Zhu, Chao F. Daniels and James Winkelman.  
MBT Timing Detection and its Closed-Loop Control Using In-Cylinder Ionization  
Signal  
Technical paper 2004-01-2976, Society of Automotive Engineers (SAE), 2004.
- [6] G.M. Rassweiler and L. Withrow.  
Motion pictures of engine flames correlated with pressure cards.  
Technical paper 800131, Society of Automotive Engineers (SAE), 1938.
- [7] R.B. Krieger and G.L. Borman.  
The computation of apparent heat release for internal combustion engines.  
ASME, 1967
- [8] F.A. Matekunas.  
Modes and measures of cyclic combustion variability.  
Technical paper 830337, Society of Automotive Engineers (SAE), 1983.

- [9] J.A. Gatowski, E.N. Balles, K.M. Chun, F.E. Nelson, J.A. Ekchian, and J.B. Heywood.  
Heat release analysis of engine pressure data.  
Technical paper 841359, Society of Automotive Engineers (SAE), 1984.
- [10] Marcus Klein.  
A Specific Heat Ratio Model and Compression Ratio Estimation  
Licentiate thesis, Vehicular Systems. LiU-TEK-LIC-2004:33, Thesis No 1104, 2004.
- [11] D. R. Lancaster, R.B. Krieger, and J.H. Lienesch.  
Measurement and analysis of engine pressure data.  
Technical paper 750026, Society of Automotive Engineers (SAE), 1975.
- [12] Lars Eriksson.  
Spark Advance Modeling and Control  
PhD thesis. Linköping Studies in Science and Technology. Dissertations No. 580.  
Linköping University, 1999.
- [13] Michael Bargende.  
Schwerpunkt-kriterium und automatische klingelerkennung.  
Motor Technische Zeitschrift, Vol 56(10):632-638, 1995
- [14] Guoming G. Zhu, Chao F. Daniels and James Winkelman.  
MBT Timing Detection and its Closed-Loop Control Using In-Cylinder Pressure Signal  
Technical paper 2003-01-3266, Society of Automotive Engineers (SAE), 2003.
- [15] André Saitzkoff, Raymond Reinmann, Thomas Berglind, and Magnus Glavmo.  
An ionization equilibrium analysis of the spark plug as an ionization sensor.  
Technical paper 960337, Society of Automotive Engineers (SAE), 1996.
- [16] André Saitzkoff, Raymond Reinmann, F. Mauss, and Magnus Glavmo.  
In-cylinder pressure measurements using the spark plug as an ionization sensor  
Technical paper 970857, Society of Automotive Engineers (SAE). 1997.
- [17] Chao F. Daniels.  
The comparison of mass fraction burned obtained from the cylinder pressure signal and spark plug ion signal.  
Technical paper 980140, Society of Automotive Engineers (SAE), 1998.
- [18] Raymond Reinmann, André Saitzkoff, and F. Mauss.  
Local air-fuel ratio measurements using the spark plug as an ionization sensor.  
Technical paper 970856, Society of Automotive Engineers (SAE), 1997.
- [19] Magnus Hellring, Thomas Munther, Thorsteinn Rögnvaldsson, Nicholas Wickström, Christian Carlsson, Magnus Larsson and Jan Nytoft  
Robust AFR Estimation Using the Ion Current and Neural Networks  
Technical paper 991161, Society of Automotive Engineers (SAE), 1999.

- 
- [20] Raymond Reinmann, André Saitzkoff, Bengt Lassesson, Petter Strandh.  
Fuel and Additive Influence on the Ion Current  
Technical paper 980161, Society of Automotive Engineers (SAE), 1998.
- [21] Axel Franke, Patrik Einewall, Raymond Reinmann and Anders Larsson.  
Analysis of the Ionization Equilibrium in the Post-Flame Zone.  
Technical paper 2003-01-0715, Society of Automotive Engineers (SAE), 2003.
- [22] A. Ahmedi, Axel Franke, H.S. Soyhan, F. Mauss and B. Sundén.  
Prediction Tool for the Ion Current in SI Combustion  
Technical paper 2003-01-3136, Society of Automotive Engineers (SAE), 2003.
- [23] Nicholas Wickström, Stefan Byttner, Thorsteinn Rögnvaldsson, Magnus Hellring.  
Neural Networks for Estimating the Pressure Peak Position from the Ion Current  
Presented at Mekatronikmöte 2003, Göteborg.
- [24] Magnus Hellring and Ulf Holmberg.  
A Simple Virtual Sensor for Combustion Timing  
In Trans. of ASME: Journal of Dynamic Systems, Measurement and Control, Vol. 125, pages 462-467, 2003
- [25] S. Haykin.  
Neural Networks – A Comprehensive Foundation  
IEEE Press, 1994
- [26] Magnus Hellring and Ulf Holmberg.  
An Ion Current Based Peak-Finding Algorithm for Pressure Peak Position Estimation  
Technical paper 2000-01-2829, Society of Automotive Engineers (SAE), 2000.
- [27] Magnus Hellring and Ulf Holmberg.  
A Comparison of Ion Current Based Algorithms for Peak Pressure Position Control  
Technical paper 2001-01-1920, Society of Automotive Engineers (SAE), 2001.
- [28] Patrick Rundin.  
Evaluation of a statistical method to use prior information in the estimation of combustion parameters  
Technical report, Vehicular Systems. LITH-ISY-EX--06/3721--SE, 2006.